Numerical computation of nonlinear normal modes in mechanical engineering

Ludovic Renson, Gaëtan Kerschen, Bruno Cochelin

▶ **To cite this version:**

Ludovic Renson, Gaëtan Kerschen, Bruno Cochelin. Numerical computation of nonlinear normal modes in mechanical engineering. Journal of Sound and Vibration, 2016, 10.1016/j.jsv.2015.09.033 . hal-01380577

HAL Id: hal-01380577
https://hal.science/hal-01380577v1

Submitted on 14 Oct 2016

HAL is a multi-disciplinary open access archive for the deposit and dissemination of scientific research documents, whether they are published or not. The documents may come from teaching and research institutions in France or abroad, or from public or private research centers.

L'archive ouverte pluridisciplinaire **HAL**, est destinée au dépôt et à la diffusion de documents scientifiques de niveau recherche, publiés ou non, émanant des établissements d'enseignement et de recherche français ou étrangers, des laboratoires publics ou privés.

Numerical Computation of Nonlinear Normal Modes in Mechanical Engineering

L. Renson[1], G. Kerschen[1], B. Cochelin[2]

[1]Space Structures and Systems Laboratory,
Department of Aerospace and Mechanical Engineering,
University of Liège, Liège, Belgium.
[2] LMA, Centrale Marseille,
CNRS UPR 7051, Aix-Marseille Université,
F-13451 Marseille Cedex, France.

Corresponding author: L. Renson
Email: l.renson@ulg.ac.be, phone: +32 4 3664854.

Abstract

This paper reviews the recent advances in computational methods for nonlinear normal modes (NNMs). Different algorithms for the computation of undamped and damped NNMs are presented, and their respective advantages and limitations are discussed. The methods are illustrated using various applications ranging from low-dimensional weakly nonlinear systems to strongly nonlinear industrial structures.

Keywords: nonlinear normal modes, numerical methods, periodic orbits, invariant manifolds, numerical continuation.

1 Introduction

The goal of modal analysis is to determine, either numerically or experimentally, the natural frequencies and vibration modes of a structure [1]. It is routinely used in industry during the design and certification process. For instance, for aircraft structures, modal parameters identified during ground vibration tests are compared to the modal parameters predicted by the numerical model in order to validate the model for subsequent flutter calculations [2].

If they are often ignored or overlooked during the design stage, structural nonlinearities are commonly encountered during test campaigns (e.g., for the Airbus A400M [3] and for the F-16 aircraft [4]). On the one hand, the presence of nonlinearity poses important challenges as novel dynamical phenomena with no linear counterpart may be observed. On the other hand, a recent body of literature reported that nonlinearity creates new opportunities for enhancing system performance. Nonlinearity was therefore deployed deliberately in acoustic switches and rectifiers [5], micromechanical oscillators [6], granular media [7], vibration absorbers [8] and energy harvesters [9].

In this context, there is a clear need for extending the linear modal analysis framework to nonlinear systems. Unlike linear modes, nonlinear normal modes (NNMs) are not orthogonal to each other, do not decouple the equations of motion and cannot be used for modal superposition. Their usefulness could therefore be questioned by the practitioner. However, important dynamical phenomena such as modal interactions between widely-spaced modes [10] and mode bifurcations [11] cannot be explained by linear theory. Up-to-date linear experimental modal analysis methods can also be challenged by nonlinearity and can, in certain cases, identify two linearized modes when only one nonlinear mode is actually excited [12]. This is why we believe that the NNM theory is an important addition to the structural dynamicist's toolbag.

The first attempts to compute NNMs were analytical [11, 13–16], and allowed to uncover the dynamical mechanisms underlying the frequency-energy dependence, interactions and bifurcations of NNMs. However, analytical methods do not lend themselves to the analysis of complex high-dimensional structures. With the advances in computing power and in computer methods (in particular in numerical continuation [17–21]), the last decade witnessed the development of numerical methods dedicated to NNMs. This research area has not yet reached maturity, but there now exist algorithms that can be effectively applied to real engineering structures, providing the kind of in-depth analysis that is required for a rigorous treatment of nonlinear systems. If reviews of the theory and applications of NNMs were recently published [22–24], the present paper is the first paper that performs a detailed and critical assessment of the different families of computational methods both for undamped and damped NNMs.

The paper is organized as follows. The two main definitions of NNMs together with their frequency-energy dependence are briefly reviewed in Section 2. Section 3 describes numerical methods that compute periodic motions of Hamiltonian systems, i.e., undamped NNMs. Section 4 discusses the computation of damped NNMs defined as two-dimensional invariant manifolds in phase space. Each section concludes with a critical assessment of the presented methods. Finally, Section 5 draws the conclusion of the paper and highlights the open problems and challenges that should drive the development of nonlinear modal analysis in the years to come.

The subject of numerical computation of periodic solutions and manifolds is extremely broad, and an extensive literature exists (see, e.g., [25–33]). A great number of methods used for NNM computation were borrowed from this body of literature. This is, for instance, the case of shooting and pseudo-arclength continuation described in Section 3 and of the trajectory-based method in Section 4.2.1. We stress that this paper focuses on the subject of NNMs and their application in mechanical engineering. There is therefore no attempt to review the developments and other applications of these methods, e.g., for the computation of forced responses and invariant manifolds of general nonlinear systems.

2 Definition and Frequency-Energy Dependence of NNMs

The foundations which served as the cornerstone of the development of the nonlinear normal mode (NNM) theory were laid down by Lyapunov and Poincaré. In his *center theorem*, Lyapunov stated that, under some regularity assumptions and non-resonance conditions, a finite-dimensional Hamiltonian system possesses different families of periodic solutions around the stable equilibrium point of the system that can be interpreted as nonlinear extensions of the normal modes of the underlying linear system [34, 35]. Based on this theoretical framework, Rosenberg defined an undamped NNM as a *vibration in unison* of the system (i.e., a synchronous periodic oscillation). This definition requires that all material points of the system reach their extreme values and pass through zero simultaneously. It allows all displacements to be expressed in terms of a single reference displacement. Rosenberg was also the first to propose constructive techniques for the calculation of NNMs [36–38]. However, this definition cannot account for modal interactions during which the periodic motion contains the frequencies of at least two interacting modes. An extended definition considering NNMs as *(non-necessarily synchronous) periodic motions* was therefore proposed in [39]; it is the definition of an undamped NNM that is considered throughout this review paper.

In view of the frequency-energy dependence of nonlinear oscillations, the frequencies, modal shapes and periodic motions of NNMs depend on the system's energy, i.e., the sum of kinetic and potential energies. For illustration, Figure 1(a) represents the backbone curve of the in-phase and out-of-phase NNMs of the two-degree-of-freedom (DOF) system

$$\begin{aligned} \ddot{x}_1 + (2x_1 - x_2) + 0.5\,x_1^3 &= 0 \\ \ddot{x}_2 + (2x_2 - x_1) &= 0 \end{aligned} \tag{1}$$

for increasing energies. The NNM motions at low energy resemble those of the corresponding mode of the underlying linear system. The modal shape is a line, and the periodic motion in phase space is an ellipse. For higher energies, the modal shape becomes a curve, and the motion in phase space turns into a deformed ellipse. Due to the hardening characteristic of the cubic spring, the period of the motion decreases for increasing energies.

If the energy is increased further for the in-phase NNM, as in Figure 1(b), other branches of periodic solutions emanate from the backbone curve. They represent the realization of $n:m$ interactions between the in-phase and out-of-phase modes. The appearance of these modal interactions is explained in Figure 2, which depicts the ratio between the frequencies of the out-of-phase and in-phase NNMs and shows that this ratio increases from $\sqrt{3}$ to $+\infty$. When the ratio is, e.g., 3, the frequency of the third harmonics of the in-phase mode is equal to the frequency of the fundamental harmonics of the out-of-phase mode, thereby realizing the condition for a 3:1 resonance between these modes. From Figure 2, one realizes that system (1) possesses a countable infinity of modal interaction branches [22]. In view of the engineering relevance of such interactions, *the overall objective of NNM*

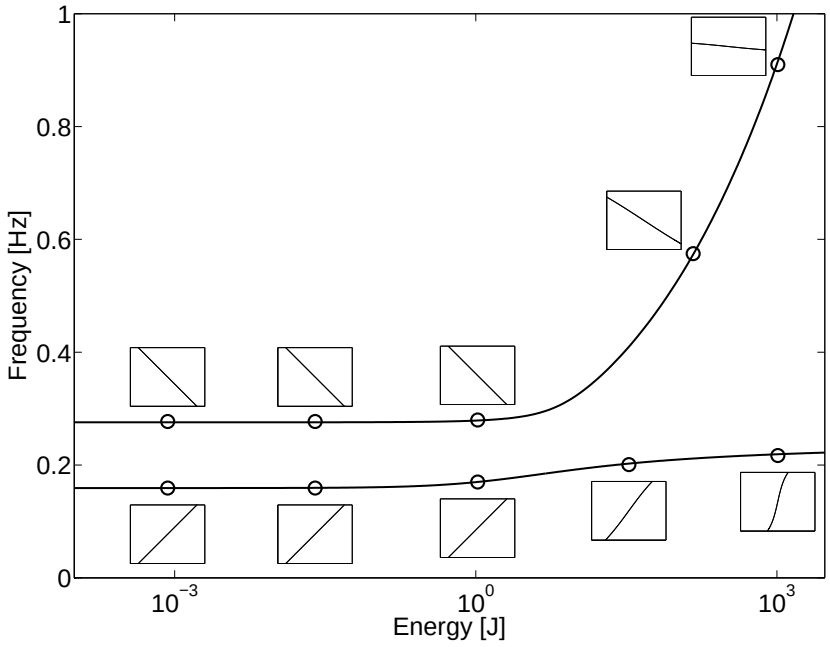

(a)

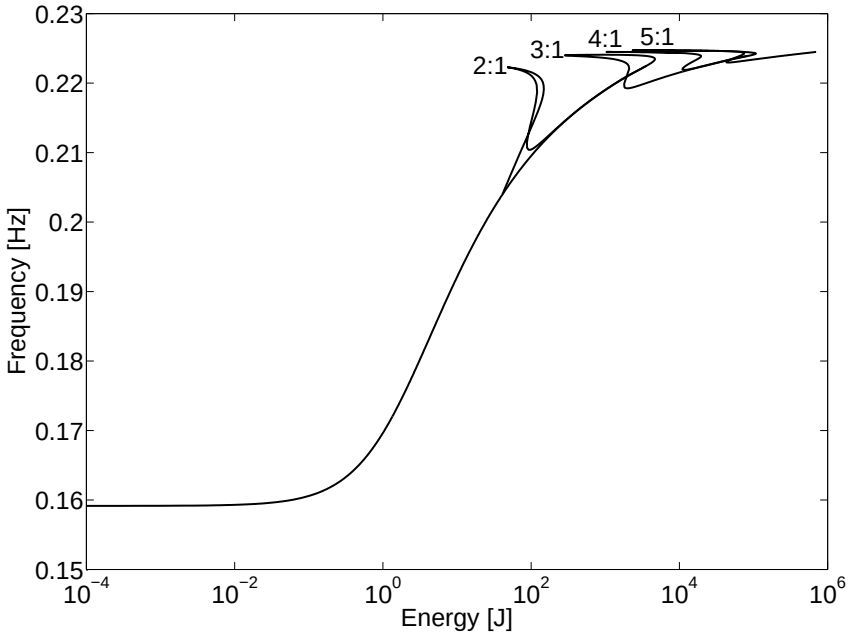

(b)

Figure 1: NNMs of system (1). (a) Frequency-energy dependence of in-phase and out-of-phase NNMs defined as periodic motions. The insets illustrate the NNM shape in the configuration space. The horizontal and vertical axes are the displacements of the first and second DOFs, respectively; (b) backbone of the in-phase NNM and modal interaction branches.

computation should therefore be to trace out both the backbone and modal interaction branches in a frequency-energy plot (FEP).

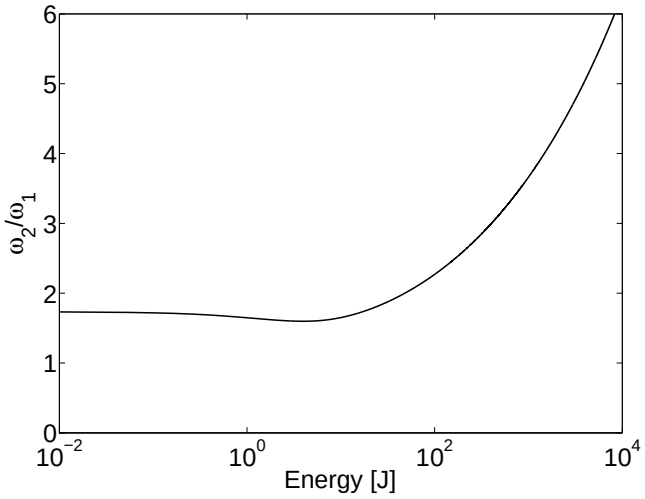

Figure 2: Ratio between the frequencies of the out-of-phase and in-phase NNMs.

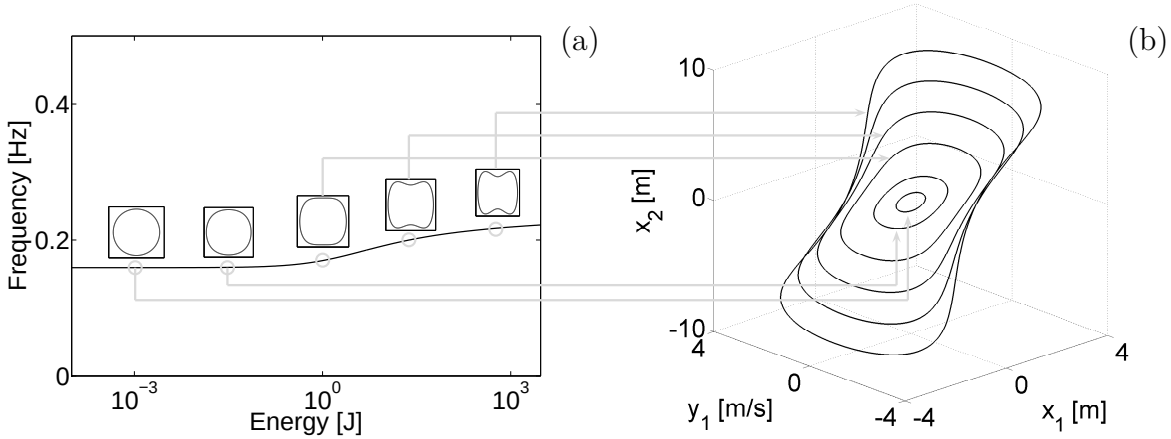

Figure 3: In-phase NNM of system (1). (a) Frequency-energy dependence of the NNM defined as periodic solutions. NNM motions in the phase plane of the first DOF are inset; (b) the NNM defined as a two-dimensional invariant manifold in phase space is paved by the collection of periodic orbits.

Even if the damped dynamics of a nonlinear system can often be interpreted based on the NNMs of the underlying undamped system, as discussed in [22], NNMs can no longer be defined as periodic motions in the presence of damping. Using geometric arguments, Shaw and Pierre proposed an elegant extension of the NNM definition to damped systems. Interpreting linear modes as invariant planes in phase space, they defined NNMs as *two-dimensional surfaces, termed invariant manifolds*, that are tangent to the linear planes at the equilibrium point [40, 41]. Generalizing the property of invariance of LNMs, such manifolds are invariant under the flow, i.e., trajectories that start out in the manifold remain in it for all time, and the system behaves as a nonlinear single-degree-of-freedom system on the manifold. In the undamped case, invariant manifolds can be constructed by simply gathering the periodic orbits defining undamped NNMs in phase space, as

in Figure 3. This figure illustrates the direct link that exists between the two NNM definitions.

Aiming at unifying the notion of periodic motion and invariance in a single definition of NNMs, Ardeh et al. [42, 43] recently introduced the concept of instantaneous center manifolds (ICMs). ICMs are defined as two-dimensional invariant manifolds containing all possible periodic orbits of the system. Essentially similar to the manifold introduced by Shaw and Pierre for conservative systems, ICMs are however restricted to the periodic part of the solution in the nonconservative case.

Finally, we remark that NNM motions can undergo bifurcations and stability changes. The description of these phenomena is beyond the scope of this paper, but the interested reader can refer to [11, 22] for further details.

3 NNMs Defined as Periodic Solutions

Assuming that continuous systems were spatially discretized, the ordinary differential equations governing the free response of a conservative mechanical system with N DOFs are

$$\mathbf{M}\,\ddot{\mathbf{x}}(t) + \mathbf{K}\,\mathbf{x}(t) + \mathbf{f}_{\text{nl}}\left(\mathbf{x}(t)\right) = 0 \tag{2}$$

where $\mathbf{M}$ and $\mathbf{K}$ are the linear mass and stiffness matrices, respectively; $\mathbf{x}$ and $\ddot{\mathbf{x}}$ are the displacement and acceleration vectors, respectively; $\mathbf{f}_{\text{nl}}$ is the nonlinear restoring force vector.

The equations of motion (2) are recast into state space form

$$\dot{\mathbf{z}} = \mathbf{g}(\mathbf{z}) \tag{3}$$

where $\mathbf{z} = [\mathbf{x}^* \quad \dot{\mathbf{x}}^*]^*$ is the $2N$-dimensional state vector, $(.)^*$ denotes the transpose operation, and

$$\mathbf{g}(\mathbf{z}) = \begin{pmatrix} \dot{\mathbf{x}} \\ -\mathbf{M}^{-1}\left[\mathbf{K}\mathbf{x} + \mathbf{f}_{\text{nl}}(\mathbf{x})\right] \end{pmatrix} \tag{4}$$

is the vector field. The solution to dynamical system (3) for initial conditions $\mathbf{z}(0) = \mathbf{z}_0 = [\mathbf{x}_0^* \quad \dot{\mathbf{x}}_0^*]^*$ is written as $\mathbf{z}(t) = \mathbf{z}\left(t, \mathbf{z}_0\right)$ in order to exhibit the dependence on the initial conditions (ICs), $\mathbf{z}\left(0, \mathbf{z}_0\right) = \mathbf{z}_0$.

Defining NNMs as families of periodic oscillations of Eqs. (3) is appealing because there exists a solid computational framework for tracing out one-dimensional families of periodic orbits [29]. Algorithms for computing undamped NNMs combine two types of methods that can be chosen independently from each other, namely (i) methods seeking isolated periodic motions and (ii) continuation methods following the family of periodic solutions corresponding to a NNM. The most popular methods are presented in Sections 3.1 and 3.2, respectively.

3.1 Computation of Isolated Periodic Solutions

A periodic solution $\mathbf{z}_p(t)$ of the autonomous system (3) is a solution that satisfies $\mathbf{z}_p(t, \mathbf{z}_{p0}) = \mathbf{z}_p(t+T, \mathbf{z}_{p0})$, where T, the minimal period, and $\mathbf{z}_{p0}$, the ICs, are *a priori* unknown. Such a solution can be described using an equation $\mathbf{H}(\mathbf{z}_p(t), T) = \mathbf{0}$ that accounts for the equations of motion (3) and expresses the closure of the orbit in state space. To define a unique solution, an additional condition, termed the phase condition, must be added. Indeed, if $\mathbf{z}_p(t)$ is a periodic solution of (3), then $\mathbf{z}_p(t + \Delta t)$ is geometrically the same solution in state space for any Δt. Hence, a condition $h(\mathbf{z}_p(t)) = 0$ should be specified to remove the arbitrariness of the initial conditions. Different phase conditions were presented in the literature [19], but a straightforward approach consists in setting one initial velocity to zero [19, 44].

In summary, an isolated NNM motion is computed by solving the augmented problem

$$\begin{cases} \mathbf{H}(\mathbf{z}_p(t), T) &= 0, \\ h(\mathbf{z}_p(t)) &= 0. \end{cases} \tag{5}$$

There exist two main approaches for defining $\mathbf{H}$. The first approach finds the ICs and the period that define the periodic orbit. This is, for instance, the case of the shooting method presented in Section 3.1.1. The second approach matches the solution of the equations of motion with shape functions and discretizes the problem using, e.g., a weighted-residual approach. The latter method describes mathematically the shape of the entire orbit which is in contrast with the former method that is only interested in a single point along the trajectory.

3.1.1 Shooting Methods

The shooting method is a popular numerical technique which iteratively finds the ICs $\mathbf{z}_{p0}$ and the period T that realize both the periodic motion and the phase condition (see, e.g., [39]). Specifically, shooting defines $\mathbf{H} = \mathbf{0}$ as a two-point boundary-value problem using the periodicity condition

$$\mathbf{H}(\mathbf{z}_{p0}, T) \equiv \mathbf{z}_p(T, \mathbf{z}_{p0}) - \mathbf{z}_{p0} = \mathbf{0} \tag{6}$$

The shooting function $\mathbf{H}(\mathbf{z}_0, T) = \mathbf{z}(T, \mathbf{z}_0) - \mathbf{z}_0$ represents the difference between the initial and final states of the system at time T.

Starting from some assumed initial conditions $\mathbf{z}_{p0}^{(0)}$, the motion $\mathbf{z}_p^{(0)}(t, \mathbf{z}_{p0}^{(0)})$ at the assumed period $T^{(0)}$ is obtained by numerical time integration of the equations of motion. Any standard technique such as Runge-Kutta algorithms can be exploited. In Ref. [44], Peeters et al. employed Newmark's method which is particularly effective for solving large-scale second-order ordinary differential equations such as those met after the finite element discretization of mechanical systems. In Ref. [45], the discrete energy-momentum method introduced by Simo and Tarnow [46] was exploited. The method has the advantage of rigorously preserving the energy between two successive time steps.

In general, the initial guess $(\mathbf{z}_{p0}^{(0)}, T^{(0)})$ does not satisfy the periodicity condition (6) and corrections to both $\mathbf{z}_{p0}^{(0)}$ and $T^{(0)}$ are sought. In Ref. [47], Slater used a general optimization algorithm to modify the initial conditions. More recently, Peeters et al. [44] used a Newton-Raphson iteration scheme to converge to the actual solution. The corrections $\Delta\mathbf{z}_{p0}^{(k)}$ and $\Delta T^{(k)}$ at iteration k are found by expanding the nonlinear function

$$\mathbf{H}\left(\mathbf{z}_{p0}^{(k)} + \Delta\mathbf{z}_{p0}^{(k)}, T^{(k)} + \Delta T^{(k)}\right) = \mathbf{0} \tag{7}$$

in a Taylor series

$$\mathbf{H}\left(\mathbf{z}_{p0}^{(k)}, T^{(k)}\right) + \left.\frac{\partial \mathbf{H}}{\partial \mathbf{z}_{p0}}\right|_{(\mathbf{z}_{p0}^{(k)}, T^{(k)})} \Delta\mathbf{z}_{p0}^{(k)} + \left.\frac{\partial \mathbf{H}}{\partial T}\right|_{(\mathbf{z}_{p0}^{(k)}, T^{(k)})} \Delta T^{(k)} + \text{H.O.T.} = \mathbf{0} \tag{8}$$

and neglecting higher-order terms (H.O.T.). As evidenced in Eqs. (8), the shooting method requires the partial derivatives of $\mathbf{H}(\mathbf{z}_0, T)$. The $2N \times 1$ vector $\partial\mathbf{H}/\partial T$ is given by

$$\frac{\partial \mathbf{H}}{\partial T}(\mathbf{z}_0, T) = \left.\frac{\partial \mathbf{z}(t, \mathbf{z}_0)}{\partial t}\right|_{t=T} = \mathbf{g}(\mathbf{z}(T, \mathbf{z}_0)). \tag{9}$$

The $2N \times 2N$ matrix $\partial\mathbf{H}/\partial\mathbf{z}_0$ follows

$$\frac{\partial \mathbf{H}}{\partial \mathbf{z}_0}(\mathbf{z}_0, T) = \left.\frac{\partial \mathbf{z}(t, \mathbf{z}_0)}{\partial \mathbf{z}_0}\right|_{t=T} - \mathbf{I}^{2N\times 2N} \tag{10}$$

where $\mathbf{I}$ is the identity matrix. The monodromy matrix $\left.\frac{\partial \mathbf{z}(t,\mathbf{z}_0)}{\partial \mathbf{z}_0}\right|_{t=T}$ represents the variation of the solution after time T when initial conditions $\mathbf{z}_0$ are perturbed. There are basically two means of computing this matrix:

1. It can be evaluated through a numerical finite difference analysis by perturbing successively each initial condition and integrating the equations of motion in time [19, 48]. This approximate method relies on extensive numerical simulations and may be computationally intensive for large-scale finite element models.

2. An alternative computation is obtained by sensitivity analysis. Differentiating the equations of motion (3) with respect to initial conditions $\mathbf{z}_0$, the monodromy matrix is governed by the linear matrix differential equation

$$\frac{d}{dt}\left[\frac{\partial \mathbf{z}(t, \mathbf{z}_0)}{\partial \mathbf{z}_0}\right] = \left.\frac{\partial \mathbf{g}(\mathbf{z})}{\partial \mathbf{z}}\right|_{\mathbf{z}(t,\mathbf{z}_0)} \left[\frac{\partial \mathbf{z}(t, \mathbf{z}_0)}{\partial \mathbf{z}_0}\right]. \tag{11}$$

   at $t = T$. It can therefore be computed by numerical integration of (11) with unit initial conditions. The reduction of the computational burden with respect to finite differences is very significant for large-scale models. In Ref. [44], the solution of equations (11) is computed together with the solution of the nonlinear equations of motion (3) in a single numerical simulation. As a result, the computation of the monodromy matrix requires only a single additional iteration at each time step, which further decreases the computational cost.

The eigenvalues of the monodromy matrix are the Floquet multipliers which dictate the stability of the NNM motions. Floquet multipliers with an amplitude greater than 1 indicate unstable motion.

3.1.2 Discretization Methods

As opposed to shooting methods which rely on time integration, discretization approaches approximate a periodic solution using trial (or, equivalently, shape) functions and transform the problem of finding a periodic orbit into solving a system of nonlinear algebraic equations. More precisely, a trajectory $\mathbf{z}(t)$ on the time interval $[0, T]$ is approximated using the series

$$\mathbf{z}(t) = \sum_{i=1}^{n_\rho} \rho_i(t)\mathbf{z}_i \tag{12}$$

where the ρ_i's and the $\mathbf{z}_i$'s are trial functions and unknown coefficients, respectively. Using a weighted residual approach, the equations of motion write

$$\int_0^T (\dot{\mathbf{z}} - \mathbf{g}(\mathbf{z}))\delta\mathbf{z}\ dt = \mathbf{0} \tag{13}$$

where the variation $\delta\mathbf{z}$ is described as

$$\delta\mathbf{z}(t) = \sum_{i=1}^{n_\psi} \psi_i(t)\delta\mathbf{z}_i \tag{14}$$

where the ψ_i's are the so-called test functions. Equations (13) have to be satisfied for arbitrary $\delta\mathbf{z}$, leading to a set of nonlinear algebraic equations that has the general form

$$\mathbf{H}(\mathbf{z}_1, ..., \mathbf{z}_{n_\rho}, T) = \mathbf{0} \tag{15}$$

Unlike Eqs. (6), Eqs. (15) only define a trajectory in phase space but do not include the periodicity conditions which have to be added. Two important examples of such methods are the so-called *harmonic balance* and *orthogonal collocation* methods.

Harmonic Balance The harmonic balance (HB) method is a widely-used approach whose first applications to mechanical and electrical engineering date back to the 1960s. Trial and test functions are defined using a Fourier basis

$$\{1, \cos(\omega t), \ldots, \cos(n_H\omega t), \sin(\omega t), \ldots, \sin(n_H\omega t)\} \tag{16}$$

where $\omega = 2\pi/T$ and n_H are the angular frequency of the periodic solution and the number of harmonic components, respectively. The unknown $\mathbf{z}(t)$ is thus represented as a truncated Fourier series

$$\mathbf{z}(t) = \mathbf{z}_E + \sum_{k=1}^{n_H} \left(\cos(k\omega t)\mathbf{z}_{C_k} + \sin(k\omega t)\mathbf{z}_{S_k}\right). \tag{17}$$

The trajectory $\mathbf{z}(t)$ is periodic by definition and is forced to satisfy the condition $\mathbf{z}(T) = \mathbf{z}(0)$. Inserting (17) into the equations of motion, the weighted residual process (13) is equivalent to collecting and balancing the terms that have the same harmonic index. This yields an algebraic system of $2N(2n_H+1)$ equations for the $2N(2n_H+1)$ unknown Fourier coefficients $\mathbf{z}_E, \mathbf{z}_{C_k}, \mathbf{z}_{S_k}$:

$$\mathbf{H}(\bar{\mathbf{z}}, \omega) = \mathbf{A}(\omega)\bar{\mathbf{z}} + \mathbf{b}(\bar{\mathbf{z}}, \omega) = \mathbf{0} \tag{18}$$

where

$$\mathbf{A}(\omega) = \text{diag}\left(\mathbf{K}, \mathbf{K}-\omega^2\mathbf{M}, \mathbf{K}-\omega^2\mathbf{M}, ..., \mathbf{K}-(n_H\omega)^2\mathbf{M}, \mathbf{K}-(n_H\omega)^2\mathbf{M}\right), \quad (19)$$

$$\bar{\mathbf{z}}^* = \left(\mathbf{z}_E^*, \mathbf{z}_{C_1}^*, \mathbf{z}_{S_1}^*, ..., \mathbf{z}_{C_{n_H}}^*, \mathbf{z}_{S_{n_H}}^*\right), \quad (20)$$

and $\mathbf{b}(\bar{\mathbf{z}}, \omega)$ is the Fourier approximation of the nonlinear force vector $\mathbf{f}_{\text{nl}}(\mathbf{x})$.

Although the HB method is simple in essence, the Fourier expansion of the nonlinear force vector $\mathbf{f}_{\text{nl}}(\mathbf{x})$ can be cumbersome (or even impractical) to evaluate if nonlinearities are nontrivial or not differentiable. Several variations of the basic algorithm were proposed to overcome this shortcoming. For instance, the incremental HB method [49] balances the harmonics only for the linearized problems that appear in the continuation process. Another approach is to alternate between time and frequency domains using the Fast Fourier Transform and its inverse. This method allows one to deal with any kind of nonlinearity as the force vector $\mathbf{f}_{\text{nl}}(\mathbf{x})$ is first computed in the time domain and then transformed back to the frequency domain [50]. Finally, Cochelin and Vergez proposed in Ref. [51] a high-order frequency-based HB method which recasts system (3) into quadratic form

$$d(\dot{\hat{\mathbf{z}}}(t)) = c + l_1(\hat{\mathbf{z}}) + l_2(\hat{\mathbf{z}}, \hat{\mathbf{z}}) \quad (21)$$

where d and l_1 are linear operators and l_2 is a bilinear operator. To this end, additional (artificial) variables are often required and gathered with the state space variables $\mathbf{z}$ in the extended vector $\hat{\mathbf{z}}$. The quadratic recast allows one to rigorously and systematically derive with simple algebra the truncated Fourier series expansion of $\mathbf{f}_{\text{nl}}(\mathbf{x})$ for a large class of nonlinear systems.

An important parameter of the method is the number of harmonics n_H that is considered in the Fourier expansion. This number can be determined prior to the computation or can evolve along the branch of periodic orbits. We can distinguish between *global methods* which impose the same number of harmonics for all DOFs and *local methods* which consider an individual number of harmonics for each DOF. The latter methods are particularly convenient as all DOFs are *a priori* not submitted to the same level of nonlinear distortions. We refer to Ref. [52] for further detail about these approaches.

Unlike shooting which is inherently a time-domain approach, the monodromy matrix is not obtained as a byproduct of the HB method. Stability can however be analyzed directly in the frequency domain using Hill's method [53, 54]. An eigenvalue problem whose solutions provide a direct access to the so-called Floquet exponents (related to the Floquet multipliers) is solved to determine the stability of a periodic solution.

Orthogonal Collocation Contrary to the HB method, orthogonal collocation is a time domain method where the time interval is divided into $n_{\Delta t}$ smaller intervals $\Delta t_j = [t_j, t_{j+1}]$ (called mesh intervals) and order-p Lagrange polynomials are considered as trial functions. Equations (3) are collocated at Gauss points for each mesh interval (i.e., using a Dirac distribution as test function $\psi_i(t)$). Grouping the discretized equations of motion together with the periodicity condition, the resulting algebraic system comprises $2N(pn_{\Delta t}+1)$ equations that can be solved using a Newton-like approach. The size of this system is

much larger than for the shooting method (6) since the unknowns are the values of $\mathbf{z}(t)$ at all collocation points. Conversely, no direct numerical integration is needed.

Interestingly, the monodromy matrix can be determined using the components of the matrix that represents the discretized problem. Similarly to the shooting method, one can in turn exploit its eigenvalues to analyze the stability of a periodic solution.

3.2 Continuation of Periodic Solutions

The numerical methods presented in Section 3.1 define a periodic solution using a system of nonlinear equations with the general form $\mathbf{H}(\mathbf{q}, \lambda) = \mathbf{0}$ with $\mathbf{H}$ a vector of n_q equations, $\mathbf{q}$ a vector of n_q unknowns (e.g., $\mathbf{z}_{p0}$ or $\bar{\mathbf{z}}$) and λ a single control parameter. Introducing the extended vector $\mathbf{U} = [\mathbf{q}^* \ \lambda]^*$, the system of equations to solve writes

$$\mathbf{H}(\mathbf{U}) = \mathbf{0} \tag{22}$$

with $\mathbf{U} \in \mathbb{R}^{n_q+1}$. For each solution of system (22), and provided it is not a bifurcation point, the implicit function theorem guarantees the existence of a locally unique one-dimensional continuum of periodic solutions called a *solution branch* (or *solution family*) [18].

Continuation (or path following) is an effective approach for determining these solutions branches given any starting point. It is based on (i) a *predictor* step which finds a first guess $\bar{\mathbf{U}}$ to the solution of (22), and (ii) a *corrector* step that improves this first guess to obtain an actual solution of Eqs. (22). Existing continuation methods differ in the order of approximation that is used in the prediction and in the constraints that are imposed for the correction. There exist numerous techniques (see, for instance, Ref. [19]), but, in the context of NNM calculation, three methods were mainly exploited, namely sequential, pseudo-arclength, and asymptotic numeric continuation.

For conservative autonomous systems, the nonlinear system of equations (5) defining the periodic solutions possesses as many equations as unknowns and does not contain any extra free control parameter for the continuation. To recast the system under the form (22), the approach proposed in Ref. [29] adds an artificial damping parameter ν and searches for the periodic solutions of the dissipative system

$$\dot{\mathbf{z}} = \mathbf{g}(\mathbf{z}) + \nu \nabla \mathcal{E}(\mathbf{z}). \tag{23}$$

where $\mathcal{E}(\mathbf{z})$ is the total energy in the system. As demonstrated in [29], periodic solutions of (23) can only exist if $\nu = 0$. As such, the parameter ν will naturally appear equal to zero in the continuation process. Introducing this artificial parameter has however the advantage of transforming the continuation problem into a square problem with as many equations as unknowns. A simplified approach where linear viscous damping is used instead of $\nabla \mathcal{E}$ was considered in Ref. [45] to compute NNMs. Alternatively, the overdetermined system of equations can be solved using the Moore-Penrose pseudo-inverse as in Peeters et al. [44].

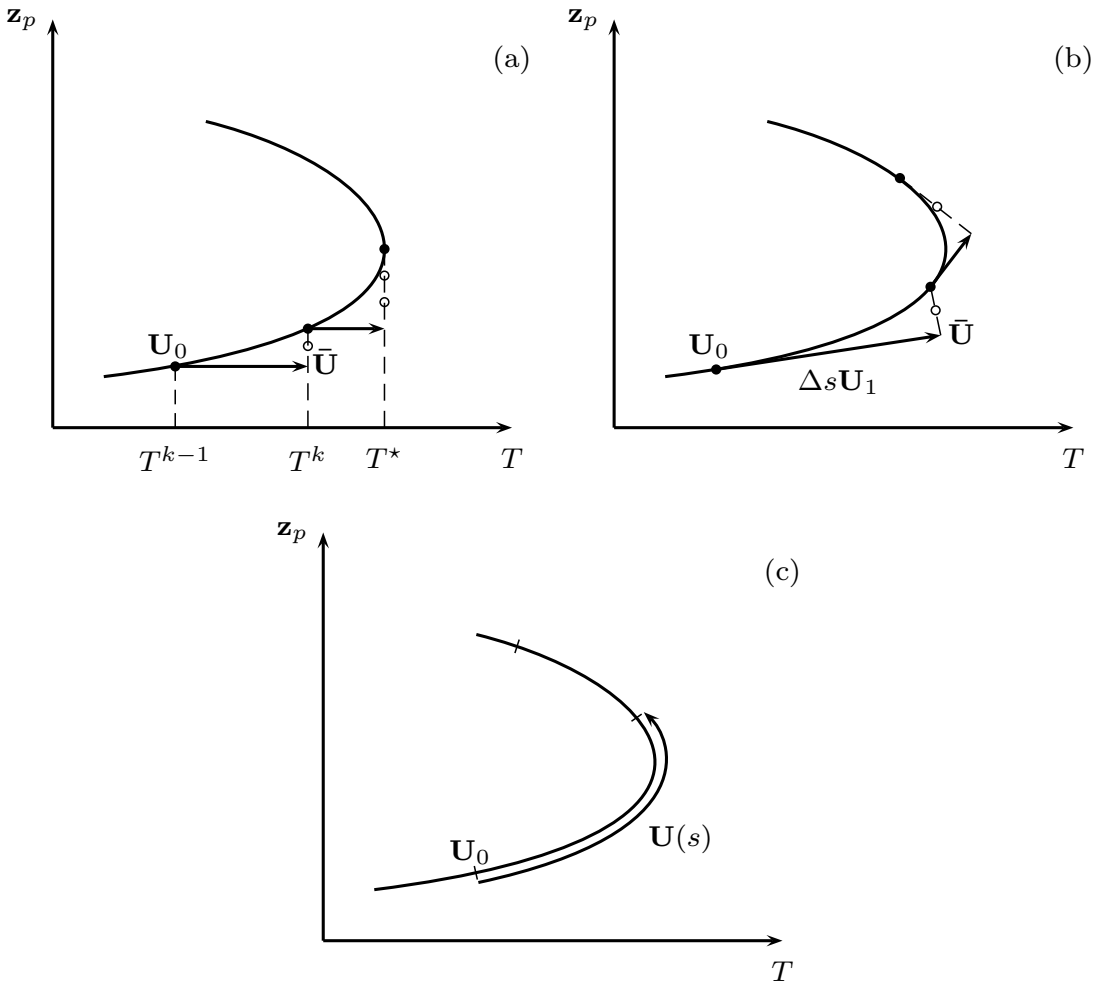

Figure 4: Schematic procedure of the predictor ($\rightarrow$) and corrector ($\circ\circ\circ$) steps followed in the (a) sequential; (b) pseudo-arclength; (c) asymptotic-numeric continuation methods. (–) Branch including a turning point.

3.2.1 Sequential Continuation

Choosing a continuation parameter U^j, sequential continuation consists of defining a zeroth-order prediction

$$\bar{U}^j = U_0^j + \Delta U^j, \tag{24}$$

$$\bar{U}^i = U_0^i \qquad \forall i \neq j, \tag{25}$$

where $\mathbf{U}_0$ is a previously-computed regular solution and ΔU^j is the increment applied to the continuation parameter. The corrector step then solves (22) while keeping $\bar{U}^j$ fixed. The principle of the method is illustrated in Figure 4(a) with the period T playing the role of the parameter U^j, as in [39].

In Ref. [47], Slater combined sequential continuation with shooting in order to increment a modal amplitude parameter and compute NNMs. Although sequential continuation is straightforward to implement, the method is limited when the solution branch presents

a turning point in parameter space. This configuration is illustrated in Figure 4(a). At $T = T^\star$, there is no solution to the problem for increasing values of T. In practice, this issue frequently occurs as, for instance, in the presence of modal interactions.

3.2.2 Pseudo-Arclength Continuation

Pseudo-arclength continuation is a first-order predictor-corrector algorithm that was first introduced by Keller [55] to systematically pass through turning points. It is arguably the most popular method for tracing out solution branches [19, 56]. Let $\mathbf{U}_0$ be a regular solution of Eqs. (22) and $\mathbf{U}_1$ the normalized tangent vector at $\mathbf{U}_0$ defined as[1]

$$\begin{array}{c} \frac{\partial \mathbf{H}}{\partial \mathbf{U}}|_{\mathbf{U}=\mathbf{U}_0}\mathbf{U}_1 = \mathbf{0}, \\ \mathbf{U}_1^*\mathbf{U}_1 = 1. \end{array} \tag{26}$$

A prediction point is computed as

$$\bar{\mathbf{U}} = \mathbf{U}_0 + \Delta s \mathbf{U}_1, \tag{27}$$

where Δs is a prescribed pseudo-arclength increment defining the distance between $\mathbf{U}_0$ and $\bar{\mathbf{U}}$ (see Figure 4(b)). Since $\bar{\mathbf{U}}$ is no longer a solution, Newton corrections are applied so as to satisfy (22) up to the required tolerance. As illustrated in Figure 4(b), imposing the Newton correction vector to be orthogonal to the tangent vector $\mathbf{U}_1$ allows the continuation method to pass through a turning point. This is a crucial requirement for NNM computation. If Δs is sufficiently small, the convergence of the Newton process is guaranteed.

3.2.3 Asymptotic Numerical Continuation

The asymptotic numerical method (ANM) relies on a high-order Taylor series expansion of the solution branch with respect to the pseudo-arclength parameter $s = \mathbf{U}_1^*(\mathbf{U} - \mathbf{U}_0)$ [58–60]. The series

$$\mathbf{U}(s) = \mathbf{U}_0 + s\mathbf{U}_1 + s^2\mathbf{U}_2 + ... + s^{n_o}\mathbf{U}_{n_o}, \tag{28}$$

where n_o typically ranges between 20 and 30, provides a local representation of the branch that passes through $\mathbf{U}_0$. Introducing (28) into a quadratic recast of the governing equations (22) as in Refs. [45, 61], the terms with the same power in s can be balanced. This leads to

$$\text{order 1:} \quad \left\{ \begin{array}{rcl} \mathbf{L}_t(\mathbf{U}_1) & = & 0, \\ \mathbf{U}_1^*\mathbf{U}_1 & = & 1, \end{array} \right. \tag{29}$$

$$\text{order } p\text{:} \quad \left\{ \begin{array}{rcl} \mathbf{L}_t(\mathbf{U}_o) & = & \mathbf{F}_p^{\text{nl}}, \\ \mathbf{U}_p^*\mathbf{U}_1 & = & 0, \end{array} \right. \tag{30}$$

[1] Alternatively, in Ref. [57], this tangent vector was approximated using $\mathbf{U}_0$ and the previously computed solution on the branch.

where $\mathbf{L}_t$ is a tangent operator and $\mathbf{F}_p^{\mathrm{nl}}$ involves the lower-order approximations $\mathbf{U}_k$ with $k \in [1, n_o - 1]$. Equations (30) can be solved sequentially for increasing orders. One advantage of this ANM continuation is that $\mathbf{L}_t$ is identical at all orders and can be inverted once for all. The computational cost of the series remains therefore limited.

The validity interval $[0, s_{max}]$ inside which the series satisfies $\|\mathbf{H}(\mathbf{U}(s))\| \leq \epsilon_r$ with ϵ_r a prescribed tolerance can be defined as [62]:

$$s_{max} = \left(\frac{\epsilon_r}{\|\mathbf{F}_{n_o+1}^{\mathrm{nl}}\|} \right)^{1/(n_o+1)} . \tag{31}$$

It is easily determined *a posteriori*. The principle of this high-order continuation is to take the end point $\mathbf{U}(s_{max})$ of the last approximation as a new starting point $\mathbf{U}_0$ for the next series development. The complete solution branch is thus known analytically as a collection of Taylor series representations. These series contain a great deal of valuable information on the solution branch which can be exploited to improve the robustness of the continuation process. For instance, any simple bifurcation point can be easily detected, and its two tangents can be captured by monitoring the emergence of geometric series in (28), referring to [63] for details.

3.3 Assessment

Shooting is one of the first methods that was used for computing NNMs numerically [47]. Since then, it was used in various applications including nonlinear beams [44,64], vibration absorbers [39, 65, 66], structures with cyclic symmetry [67], and granular chains [68]. Quite simple to implement, shooting requires moderate memory resources as the size of the Jacobian matrix of $\mathbf{H}$ is $2N \times 2N$ where N is the number of DOFs. Targeting further reduction of the computational cost, Peeters et al. [44] exploited the symmetries of fundamental NNMs. Specifically, thanks to symmetry in time, shooting can be performed over half the motion period, dividing the computational cost by a factor of two. In addition, spatial symmetry of NNMs allows for a phase condition that sets all initial velocities to zero thereby dividing the number of unknowns by two. Combined with sensitivity analysis, these improvements make shooting a suitable candidate for addressing large-scale, complex systems.

For instance, the NNMs of the Morane-Saulnier 760 aircraft, a full-scale airframe that presents softening nonlinearities in the bolted connections between the external fuel tanks and the wing tips (see Figure 5), were computed from a reduced-order model comprising 548 DOFs in [69]. Figure 6 represents the FEP of the first symmetric wing torsional mode. The oscillation frequency along the backbone undergoes a substantial decrease for increasing energies because torsion induces important deformations in the bolted connections. As for the 2DOF system presented in Section 2, the FEP of the aircraft also features branches of modal interactions. Specifically, three branches realizing 3:1, 5:1 and 9:1 internal resonances with higher-frequency modes can be observed in Figure 6. The evolution of the modal shapes along the 3:1 branch in Figures 6(a – c) depicts a smooth transition from symmetric wing torsion to a higher-frequency tail torsional mode. Both

modes are present in the linear modal basis, but their mixing shown in Figure 6(b) is not. It is therefore a mode with no linear counterpart.

(a) (b)

Figure 5: Morane-Saulnier 760 aircraft. (a) Photograph; (b) close-up of the bolted connections between the wing tip and an external fuel tank. Figure reproduced from [69].

The shooting technique was also applied to another real-life engineering application, i.e., the SmallSat spacecraft developed by EADS-Astrium. This satellite is equipped with a vibration isolation device possessing multiple lateral and axial mechanical stops [70]. Figure 7(a) presents a photograph of the structure at EADS Astrium testing facilities in Stevenage (UK). Time series recorded during a test campaign are presented in Figure 7(b). For a swept-sine base excitation of $0.1\,g$, the satellite response at the instrument panel presents a single resonance peak around 60 Hz. For a forcing amplitude of $1\,g$, another resonance peak characterized by a larger amplitude appears before 30 Hz. This is the clear manifestation of an inherently nonlinear resonance, as there is no linear mode involving instrument panel deformation in this frequency range. This finding was confirmed numerically through the computation of the sixth NNM of the spacecraft in Ref. [70]. The FEP of this mode in Figure 7(c) depicts a 2:1 modal interaction during which the second harmonics of a mode of the vibration isolation device excites a mode of the instrument panel. The modal shapes on the branch are inset in Figure 7(c). As for the aircraft, mixing between modes of the linear basis can be observed. In view of the important accelerations measured at the instrument panel, this modal interaction is of great practical relevance.

Thanks to the nonlinear phase lag quadrature criterion [71], an original computation of undamped NNMs in forced and damped systems was presented in Ref. [72]. To this end, an additional equation imposing quadrature between the applied force and the response was added to the standard shooting function (6). In Refs. [73, 74], the NNMs were computed in configuration space using a shooting function that constraints the end points of the trajectory to reach the same equipotential surface.

Shooting is *per se* limited by the capabilities of time integration algorithms. It can fail for strongly unstable systems, as reported in [19], and it hardly deals with piecewise linear or nonsmooth systems, unless specific time integration techniques or regularization are considered. An additional difficulty with shooting is that the small step sizes that are

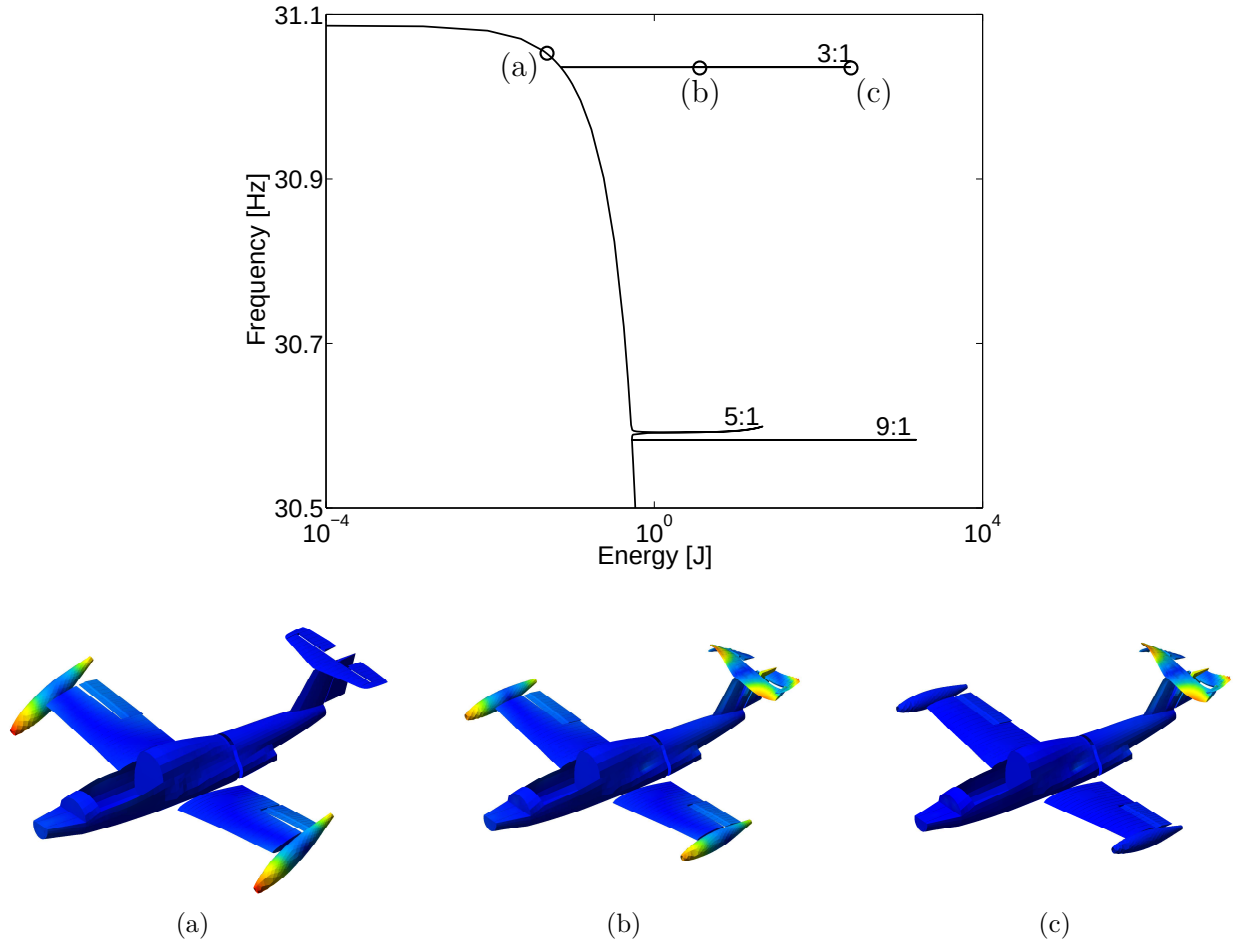

Figure 6: FEP of the first symmetric wing torsional NNM of the Paris aircraft. NNM motions (a) on the backbone (in the vicinity of the branch); (b) in the middle of the branch of 3:1 internal resonance between the first wing torsional mode and a higher tail mode; and (c) at the extremity of the branch. Figure reproduced from [69].

required for accurate time integration increase the sensitivity to high-order harmonics present in the response. As a result, numerous modal interactions, whose computations are demanding, can be encountered along a NNM branch. An illustration of this issue is presented for the fifth NNM of the satellite in Figure 8(a). The 15:1 and 120:1 modal interactions were found to be very sensitive to small perturbations, and their practical significance is therefore questionable.

Thanks to its inherent filtering properties, the HB method offers an interesting alternative to the shooting method. For linear problems, the HB method rigorously solves the equations of motion using a single harmonic ($n_H = 1$). For problems with smooth nonlinearities, experience shows that the number of harmonics required for an accurate approximation of the solution is often limited. The size of the algebraic system (18), i.e., $2N(2n_H + 1)$, remains moderate, and the method outperforms the time integration algorithms used in the shooting approach. The HB method was successfully applied to a wide variety of problems including rotor dynamic applications with mistuned bladed disks [76],

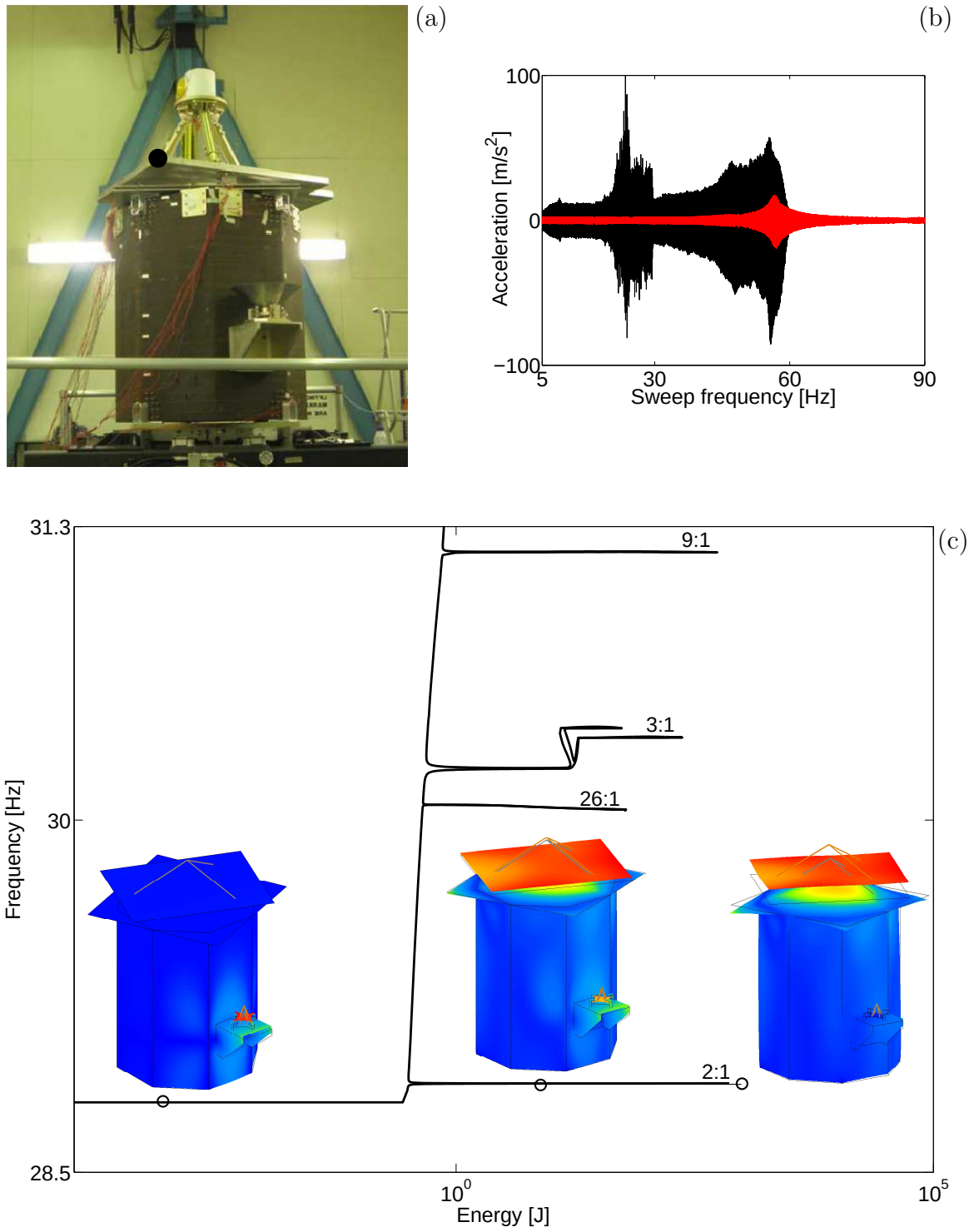

Figure 7: The SmallSat spacecraft. (a) Photograph; (b) accelerations measured at the instrument panel (black dot in Fig. 7(a)) for 0.1 g (red) and 1 g (black) swept sine base excitations; (c) sixth NNM computed using a method combining shooting and pseudo-arclength continuation. Modal shapes are inset. Figure reproduced from [70].

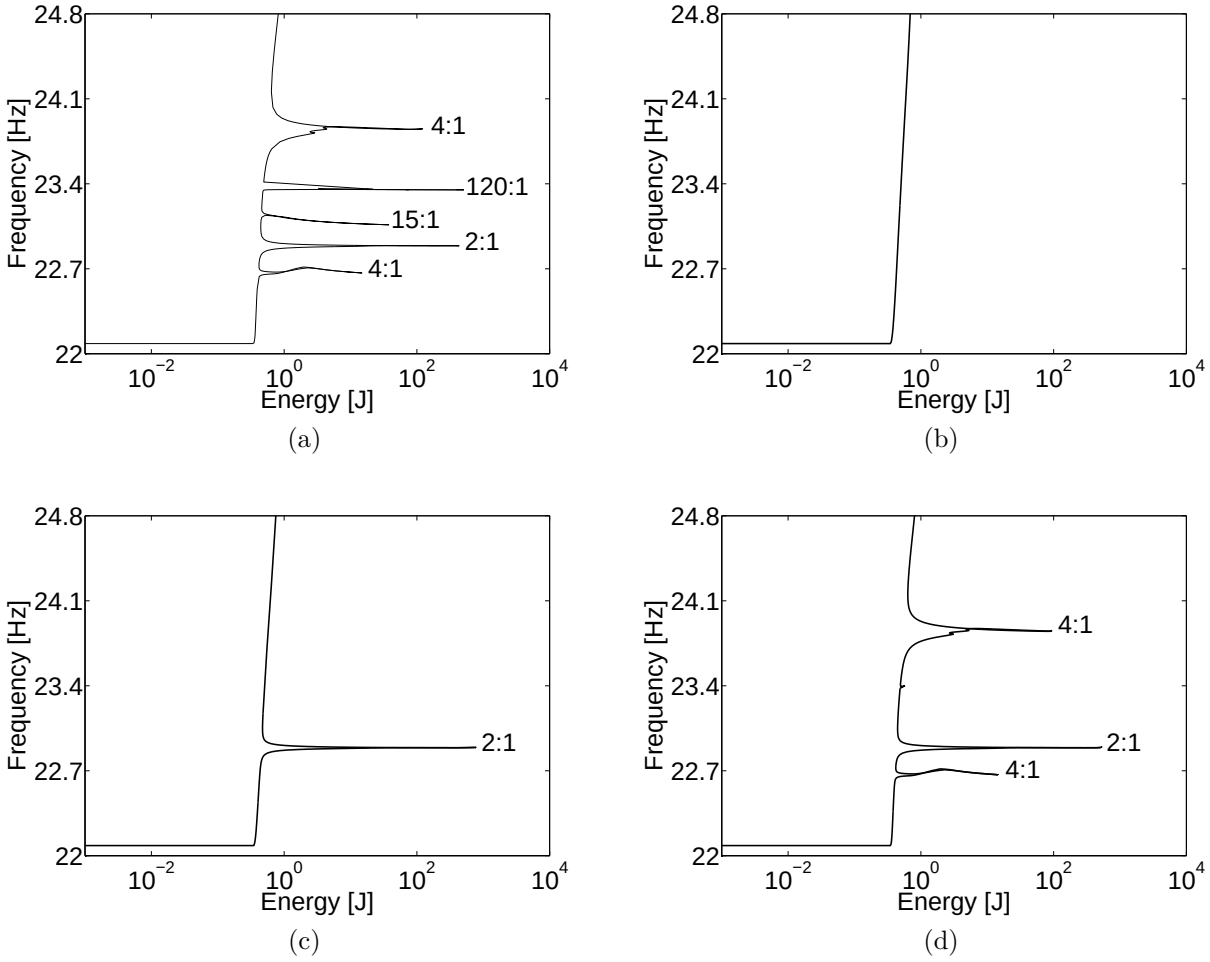

Figure 8: Fifth NNM of the SmallSat spacecraft. (a) Method combining shooting and pseudo-arclength continuation; (b-d) HB method with one, three, and five harmonics, respectively, and combined with pseudo-arclength continuation. Figure reproduced from [75].

structures with cyclic symmetry [77, 78], and vibration absorbers [79], but this is probably in the study of geometrically nonlinear systems that HB was the most extensively used [57, 80–84].

HB was used in Ref. [75] as an effective solution to the issue posed by the computation of numerous modal interactions. Figures 8(b-d) present the branch of the fifth NNM of the SmallSat spacecraft obtained by retaining one, three and five harmonics in the Fourier series, respectively. The backbone branch computed with one harmonics in the series, resulting in a very limited computational effort, is already in excellent agreement with the backbone calculated by the shooting method. The successive inclusion of higher harmonics adds a sequence of modal interaction branches. The decision of the computation of modal interactions is therefore left to the user, which is a particularly attractive feature of the HB method.

The method can also capture the dynamics of stiff nonlinear systems as, for instance, systems including regularized nonsmooth nonlinearities. Karkar analyzed the periodic regimes of a clarinet whose model includes an impact oscillator for the reed, Bernoulli's equation for the mouthpiece flow, and damped acoustic linear modes for the resonator [85, 86]. Moussi [87] computed the NNMs of a clamped simply-supported linear elastic beam connected to a bilateral nonlinear elastic contactor schematized in Figure 9(a). The FEP of the first mode is displayed in Figure 9(b). An important number of modal interactions is captured by the algorithm, because a large number of harmonics was required to accurately compute the periodic orbits of this stiff system. Interestingly, the 3:1 resonance with the second NNM forms a large loop that, unlike the aircraft and satellite examples, is not localized in a narrow frequency band. The periodic solutions corresponding to this interaction can probably be excited using larger ranges of initial conditions and frequencies. The application of the HB method to a simplified model of a steam generator present in nuclear power plants is presented in Figure 10. The vertical U-pipe transports high-pressure hot water that is directly in contact with the radioactive material of the core. The pipe is maintained in its vertical position by a strut plate that introduces gaps. The natural frequency of the first out-of-plane NNM in Figure 10(b) increases due to the hardening effect of the impacts between the pipe and the plate. Around 6 Hz, a 8:1 modal interaction couples the out-of-plane and in-plane motions of the structure. Adopting a linear design standpoint, this coupling would be ignored in view of the frequency gap between the corresponding linear normal modes. This modal coupling can jeopardize structural integrity as in the San Onofre (USA) power plant where a pipe rupture occurred after unexpected in-plane motions [88].

Orthogonal collocation is a well-established approach that is implemented in numerous software (e.g., AUTO [90] and MATCONT [91]). NNMs of a simple 2DOF system and of geometrically nonlinear plates were computed using AUTO in Refs. [92, 93], respectively. If the collocation method is accurate and can benefit from adaptive meshing strategies for the time interval [90], the method can become computationally intensive for large finite element models, due to the size of the algebraic system to solve, $2N(pn_{\Delta t}+1)$. In Ref. [89], the HB and orthogonal collocation methods were compared using the SDOF (regularized) impact oscillator illustrated in Figure 11(a). The HB method required about 200 harmonics to obtain a periodic orbit with almost no visible difference with the reference solution and was shown to exhibit the classical Gibbs phenomenon (see Figure 11(b)). The orbit obtained with orthogonal collocation in Figure 11(c) is smoother and appears to better capture the reference solution, because the continuity of the trajectory is only imposed between two successive time intervals. However, without adaptive meshing strategies, at least 202 intervals were needed to obtain one time interval during the impact time and properly capture this region. For both smooth and nonsmooth systems, Ref. [89] concluded in a better convergence of the HB method compared to orthogonal collocation.

Moving now to the assessment of methods for the continuation of periodic solutions, it is clear that sequential continuation cannot be considered as a robust algorithm. Equipped with an adaptive step-length selection strategy, the pseudo-arclength method is used in several continuation software such as, e.g., AUTO [90] or NNMcont [94]. It can trace out complex backbone and modal interaction branches, as confirmed in Figure 8. We mention that there exist other alternatives to corrections that are orthogonal to the tan-

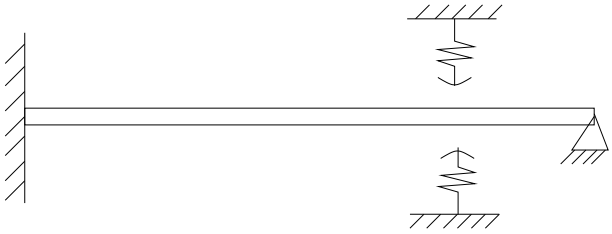

(a)

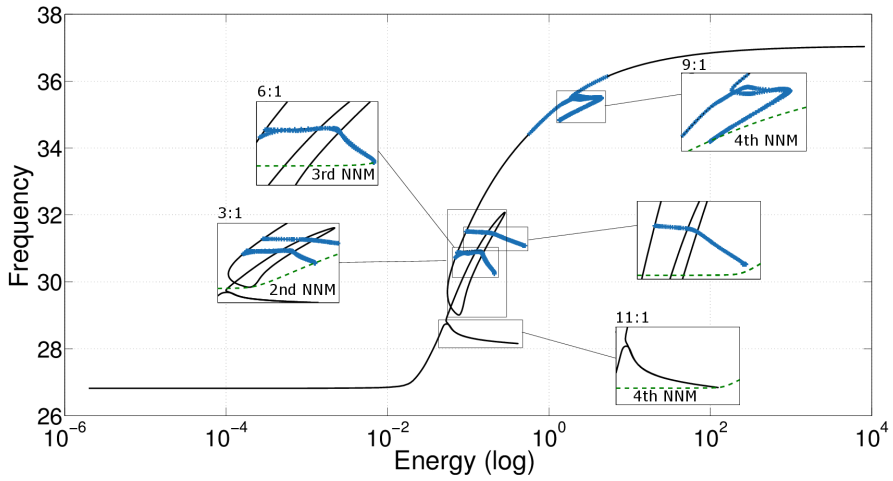

(b)

Figure 9: Clamped-simply-supported beam with a bilateral contactor. (a) Schematic of the system; (b) FEP of the first NNM. Figure reproduced from [87].

gent predictions, e.g., the Moore-Penrose scheme used in MATCONT [91]. A comparison between three correction approaches for the calculation of the NNMs of a 2DOF system is reported in [95].

The more recent ANM continuation scheme was used in different areas, including structural dynamics [96] and fluid dynamics [97, 98]. Combined with the HB method in the MANLAB software [99], ANM was used for obtaining the results presented in Figures 9 and 10. The method does not require any step-control strategy. Furthermore, the cost of this high-order method remains moderate if the original system is recast into quadratic form (as in Eqs. (21)). *A priori* cumbersome, this operation can however be replaced by automatic differentiation [100] for an automatic generation of the Taylor series. Finally, a particularly attractive feature of the method is that the resulting Taylor series can be analyzed to detect and characterize the bifurcations that occur along the branch of solutions. The robustness of the continuation algorithm is thereby preserved even in the presence of numerous internal resonances.

The present section focused on methods for computing NNMs of autonomous conservative systems but, clearly, this presentation is by no means exhaustive. For instance, two different approaches that bear strong resemblance to the methods described in Section 4 were presented in Ref. [101]. For the first method, low-amplitude initial conditions onto

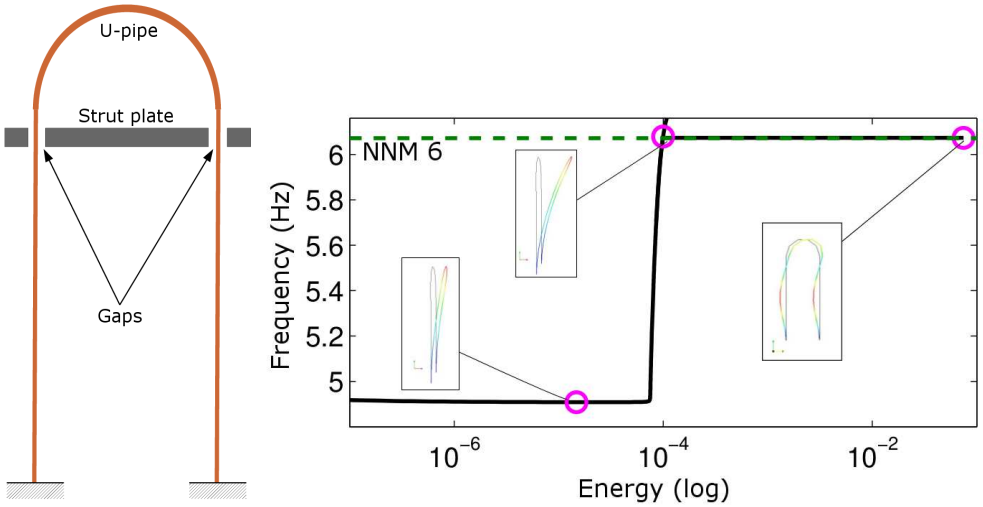

(a) (b)

Figure 10: Simplified model of a vertical U-pipe of a steam generator. (a) Schematic of the system; (b) FEP of the first out-of-plane bending mode. Figure reproduced from [87].

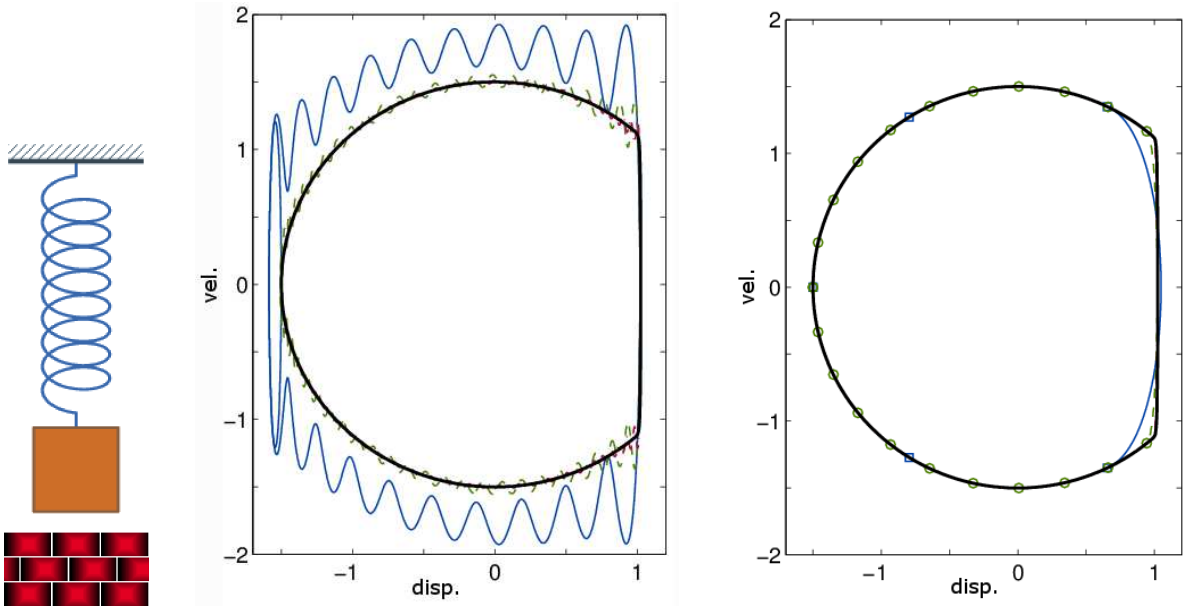

(a) (b) (c)

Figure 11: Vibro-impact system. (a) Schematic of the system; (b) phase diagram given by the HB method (blue $N_H = 20$; green $N_H = 50$, red $N_H = 100$; orange $N_H = 200$); (c) phase diagram given by orthogonal collocation (blue $n = 16$; green $n = 64$; red $n = 202$; orange $n = 400$). Figure reproduced from [89].

a LNM were considered, and small negative damping was artificially introduced into the conservative equations of motion. A trajectory spiraling out of the equilibrium point was then obtained using time integration. By virtue of the invariance property of a NNM,

this trajectory describes the NNM corresponding to the chosen LNM. In comparison with the shooting technique that also relies on time integration, this method may require very long simulations, depending on the amount of damping introduced. In addition, as we shall see in Section 4, the introduction of linear damping may strongly alter the dynamics of the conservative system. For the second method, a supplementary differential equation governing a parameter $\lambda(t)$ was appended to the conservative equations of motion in order to progressively introduce the nonlinearities into the system. Considering initial conditions on a LNM and $\lambda(0) = 0$, the curved NNM was obtained as time evolved and λ approached 1. In Ref [102], Laxalde et al. studied the first NNM of a turbomachinery blade in frictionless contact at its tip. Periodic solutions were sought by minimizing a Rayleigh quotient together with Lagrange multipliers for the contact constraints. The unknown displacements were discretized using Fourier series as in the HB method.

4 NNMs Defined as Two-Dimensional Invariant Manifolds

As reported in the literature [11], the damped dynamics of a nonlinear system can often be interpreted based on the topological structure and bifurcations of the NNMs of the underlying Hamiltonian system. However, complex damping mechanisms can be present in engineering structures, particularly in interfaces between components, and even "simple" viscous damping may sometimes drastically alter the dynamics. This is for instance the case for the 2DOF system presented in Figure 12. Previously studied in Refs. [103–106], this system contains quadratic and cubic nonlinearities arising from second-order terms in the strain tensor. Figure 13 presents the system's frequency response to harmonic excitation for different forcing amplitudes and damping levels. The forced responses were computed out using numerical continuation. For low modal damping, a hardening behavior is observed for the first resonance. As nonlinear resonances occur in the neighborhood of NNMs [11], the first NNM of the underlying conservative system provides an accurate representation of the resonance locus of the weakly damped system, as shown in Figure 13(a). However, when the modal damping ξ_2 of the second mode is increased, the hardening behavior turns unexpectedly into softening behavior. Such a fundamental change in the dynamics cannot obviously predicted by undamped NNMs. The recourse to damped NNMs is then necessary, as confirmed in Figure 13(b).

We now consider more general nonlinear autonomous equations of motion

$$\mathbf{M}\,\ddot{\mathbf{x}}(t) + \mathbf{C}\,\dot{\mathbf{x}}(t) + \mathbf{K}\,\mathbf{x}(t) + \mathbf{f}_{\text{nl}}\left(\mathbf{x}(t), \dot{\mathbf{x}}(t)\right) = \mathbf{0} \tag{32}$$

where $\mathbf{M}$ and $\mathbf{K}$ are the linear mass and stiffness matrices, respectively; $\mathbf{x}$, $\dot{\mathbf{x}}$, and $\ddot{\mathbf{x}}$ are the displacement, velocity, and acceleration vectors, respectively; $\mathbf{f}_{\text{nl}}$ is the nonlinear restoring force vector. There is no specific assumption on the matrix $\mathbf{C}$ which can have both symmetric (nonconservative) and skew-symmetric (conservative) contributions. The linear damping needs not be proportional. The system of equation (32) is transformed

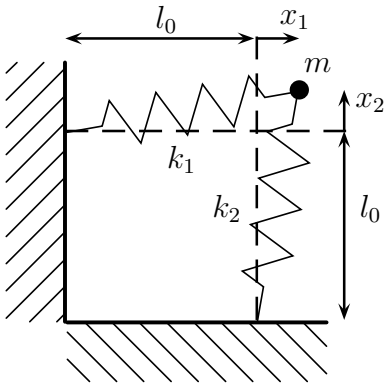

Figure 12: Schematic representation of the 2DOF example.

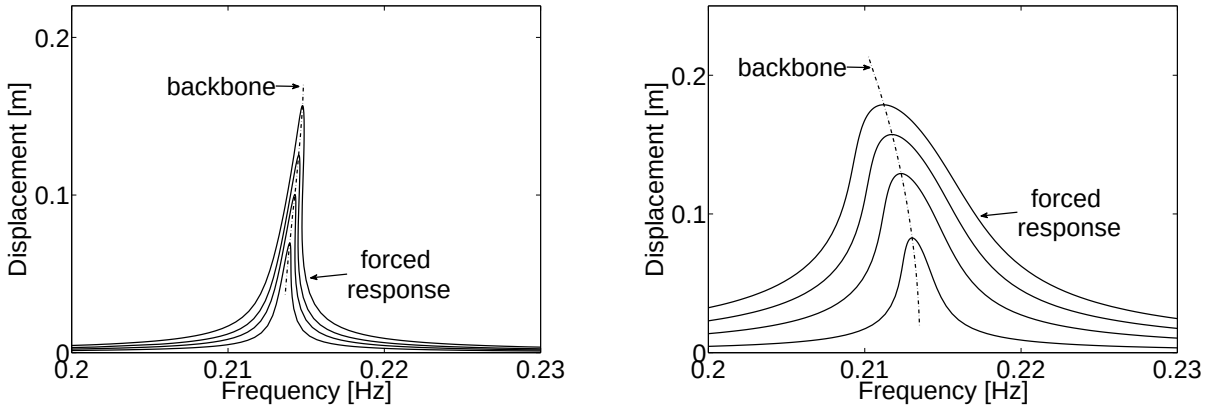

Figure 13: Harmonic response of the 2DOF damped system presented in Figure 12. (a) Low modal damping ($\xi_1 = 0.001$, $\xi_2 = 0.005$); solid line: numerical continuation; dashed line; backbone curve computed from the undamped NNM; (b) higher modal damping ($\xi_1 = 0.001$, $\xi_2 = 0.2$); solid line: numerical continuation; dashed line; backbone curve computed from the damped NNM.

into its first-order form

$$\dot{\mathbf{z}} = \mathbf{g}(\mathbf{z}) = \begin{pmatrix} \dot{\mathbf{x}} \\ -\mathbf{M}^{-1}\left[\mathbf{C}\,\dot{\mathbf{x}} + \mathbf{K}\mathbf{x} + \mathbf{f}_{\mathrm{nl}}(\mathbf{x}, \dot{\mathbf{x}})\right] \end{pmatrix} = \begin{pmatrix} \mathbf{y} \\ \mathbf{f}(\mathbf{z}) \end{pmatrix}, \tag{33}$$

where the term $\mathbf{f}$ represents all the inertia-normalized (linear and nonlinear) elastic and dissipative forces in the equations of motion.

Several methods for computing NNMs of the general system (33) were proposed in the technical literature. These methods differ in the interpretation of the definition of a NNM as a two-dimensional invariant manifold and are divided into three categories according to the mathematical problem in hand. The first methods presented in Section 4.1 solve partial differential equations (PDEs) in order to directly compute the two-dimensional surface of the manifold. Section 4.2 discusses two methods that obtain NNMs using

boundary value problems (BVPs). Finally, in Section 4.3, NNM calculation takes the form of a nonlinear eigenvalue problem and results in the computation of trajectory portions on the manifold.

4.1 The Manifold-Governing PDEs

In the general damping case, the linear theory resorts to complex LNMs to account for the phase lag between the DOFs of a system. Shaw and Pierre demonstrated that the description of a mode using a displacement-velocity pair of coordinates is, in essence, similar to this complex-valued approach. Hence, they proposed to parametrize the two-dimensional invariant manifold, or equivalently the NNM, using a single *master pair* of state-space variables, a displacement x_k and a velocity y_k, the other variables being functionally related to this master pair. The constructive approach for calculating NNMs was then inspired by the center manifold theory [107].

Writing the master coordinates as (u, v), the remaining variables follow the constraint equations

$$x_i = X_i(u, v), \qquad y_i = Y_i(u, v), \qquad i = 1, ..., N;\ i \neq k. \tag{34}$$

Similarly to the center manifold approach, the time dependence in the equations of motion is eliminated by asserting that the motion occurs on the invariant manifold. Doing so, the time derivative of Equations (34) gives

$$\dot{x}_i = \frac{\partial X_i}{\partial u}\dot{u} + \frac{\partial X_i}{\partial v}\dot{v}, \qquad \dot{y}_i = \frac{\partial Y_i}{\partial u}\dot{u} + \frac{\partial Y_i}{\partial v}\dot{v}, \tag{35}$$

where $\dot{u} = v$ and $\dot{v} = f_k$. Substituting these equations into (33) leads to a set of $2N - 2$ PDEs that have to be solved for the X_is and Y_is

$$\begin{aligned} Y_i(u, v) &= \frac{\partial X_i(u, v)}{\partial u} v + \frac{\partial X_i(u, v)}{\partial v} f_k, \\ f_i &= \frac{\partial Y_i(u, v)}{\partial u} v + \frac{\partial Y_i(u, v)}{\partial v} f_k, \end{aligned} \tag{36}$$

where $i = 1, ..., N;\ i \neq k,\ f_i = f_i(u, \mathbf{X}(u, v), v, \mathbf{Y}(u, v))$ are the components of $\mathbf{f}$ in Eq. (33) with $\mathbf{X} = \{X_j : j = 1, ..., N\ ; j \neq k\}$ and $\mathbf{Y} = \{Y_j : j = 1, ..., N\ ; j \neq k\}$.

Around the system's equilibrium point, the manifold-governing PDEs (36) admit N solutions which are the nonlinear extension of the N underlying LNMs [41]. Originally, a solution of Eqs. (36) was approximated using Taylor series expansions in (u, v). Balancing the like-power terms, a set of algebraic equations was obtained and recursively solved in order to obtain the constraint equations (34) which describe the geometry of the NNM in phase space [41].

Eventually, substituting the X_is and Y_is in the ordinary differential equations governing the master coordinates x_k and y_k, the dynamics on the NNM reduces to a SDOF oscillator governed by:

$$\begin{aligned} \dot{u} &= v, \\ \dot{v} &= f_k(u, \mathbf{X}(u, v), v, \mathbf{Y}(u, v)). \end{aligned} \tag{37}$$

4.1.1 A Galerkin-Based Approach

The first attempt to solve the PDEs (36) numerically is that of Pesheck et al. [108]. Equations of motion were first written in modal space as

$$\ddot{\boldsymbol{\eta}} + \boldsymbol{\Xi}\dot{\boldsymbol{\eta}} + \boldsymbol{\Omega}\boldsymbol{\eta} = \hat{\mathbf{f}}(\boldsymbol{\eta}, \dot{\boldsymbol{\eta}}) \tag{38}$$

with $\boldsymbol{\eta}$ the vector of normalized modal coordinates, $\boldsymbol{\Xi}$ the modal damping matrix, and $\boldsymbol{\Omega}$ the modal stiffness matrix. $\hat{\mathbf{f}}(\boldsymbol{\eta}, \dot{\boldsymbol{\eta}})$ is the nonlinear force vector projected onto the linear modal basis. Following the same two-dimensional parametrization of the invariant surface as the previous section, a pair of master variables $(\eta_k, \dot{\eta}_k)$ is chosen and the remaining coordinates are described in terms of this pair. An additional transformation into polar coordinates is used to change the master pair into an amplitude a and a phase ϕ:

$$\eta_k = a\cos\phi, \qquad \dot{\eta}_k = -a\omega_k \sin\phi. \tag{39}$$

The constraint relations are

$$\eta_i = P_i(a,\phi), \qquad \dot{\eta}_i = Q_i(a,\phi), \qquad i = 1, ..., N;\ i \neq k. \tag{40}$$

The manifold-governing PDEs are

$$\begin{aligned} Q_i &= \frac{\partial P_i}{\partial a} a\tilde{f}_k \sin\phi + \frac{\partial P_i}{\partial \phi}\left(\omega_k + \tilde{f}_k\cos\phi\right), \\ -2\zeta_i\omega_i Q_i - \omega_i^2 P_i + \hat{f}_i &= \frac{\partial Q_i}{\partial a} a\tilde{f}_k \sin\phi + \frac{\partial Q_i}{\partial \phi}\left(\omega_k + \tilde{f}_k\cos\phi\right), \end{aligned} \tag{41}$$

where $\tilde{f}_k = -\left(\frac{\hat{f}_k}{a\omega_k} + 2\zeta_k\omega_k\sin\phi\right)$ and $i = 1, ..., N;\ i \neq k$. Equations (41) can be solved in the domain $(a, \phi) = [0, A] \times [0, 2\pi]$. The phase-amplitude formulation allows to approximate the functionals P_i and Q_i with double series expansions

$$P_i(a,\phi) = \sum_{l=1}^{n_a}\sum_{m=1}^{n_\phi} c_i^{l,m}\rho_{l,m}^P(a,\phi), \qquad Q_i(a,\phi) = \sum_{l=1}^{n_a}\sum_{m=1}^{n_\phi} d_i^{l,m}\rho_{l,m}^Q(a,\phi), \tag{42}$$

where the functions $\rho_{l,m}^P$ and $\rho_{l,m}^Q$ are global shape functions. They can be split into polynomial (for the amplitude) and harmonic (for the phase) contributions as

$$\rho_{l,m}^P(a,\phi) = R_l(a)\cos((m-1)\phi), \qquad \rho_{l,m}^Q(a,\phi) = R_l(a)\sin(m\phi) \tag{43}$$

where $R_l(a)$ are orthogonal polynomial functions [108]. Introducing Equations (42) into the PDEs (41) and using a Galerkin projection based on the individual shape functions gives a set of $2(N-1)n_a n_\phi$ highly-coupled and highly-nonlinear algebraic equations that is eventually solved using a Newton-like method. To improve the computational efficiency of the method, the computational domain was divided into small strips in amplitude where linear shape functions (in amplitude) were considered to simplify the formulation [109].

4.1.2 A Transport Method

More recently, Blanc et al. [104] proposed a new method for solving (41). The PDEs were written as a transport problem:

$$\begin{aligned} \mathbf{V} \cdot \nabla P_i &= Q_i, \\ \mathbf{V} \cdot \nabla Q_i &= \hat{f}_i - \omega_i^2 P_i, \qquad i = 1, ..., N;\ i \neq k, \end{aligned} \tag{44}$$

where ∇ is the gradient operator and $\mathbf{V} = (\dot{a}, \dot{\phi})$ is a velocity vector whose components are

$$\dot{a} = -\frac{\hat{f}_k \sin\phi}{\omega_k}, \qquad \dot{\phi} = \omega_k - \frac{\hat{f}_k \cos\phi}{a\omega_k}. \tag{45}$$

To solve the transport PDEs in a domain $(a, \phi) =]0, A[\times]0, 2\pi[$ (see Figure 14), boundary conditions (BCs) are required at inflow, i.e., where the velocity vector $\mathbf{V}$ points inward the computational domain. Consequently, BCs were imposed along the zero-phase boundary and iteratively modified to obtain the continuity of the manifold, i.e., $P_i(a, 0) = P_i(a, 2\pi)$ and $Q_i(a, 0) = Q_i(a, 2\pi)\ \forall i \neq k$. The problem of finding these suitable BCs at $\phi = 0$ was written as a minimization problem. Additional BCs were also specified along the $a = A$ boundary where inflow was present.

The transport problem was solved using an off-centered finite difference (FD) scheme on a regular grid. The scheme starts at $\phi = 0$ and follows the flow of the PDEs to progress toward increasing values of ϕ. At a phase line n, the partial derivative of P (similarly of Q) in the amplitude direction was:

$$\left(\frac{\partial P}{\partial a}\right)(a_m, \phi_n) \approx \frac{P_n^m - P_n^{m-1}}{\delta a} \qquad \text{if} \quad V_a^{n,m} > 0, \tag{46}$$

$$\left(\frac{\partial P}{\partial a}\right)(a_m, \phi_n) \approx \frac{P_n^{m+1} - P_n^m}{\delta a} \qquad \text{if} \quad V_a^{n,m} < 0, \tag{47}$$

at point (a_m, ϕ_n). The choice of the discretization according to the direction of the velocity is classical for transport problems. We refer to Ref. [104] for additional details about the discretization scheme.

Eventually, the Jacobian matrix of the optimization problem was obtained by the method of the adjoint state [104, 110] and the problem was solved using a Newton-like method.

4.1.3 A Finite-Element-Based Approach

Following the simplification of the shape functions initiated in [109], Renson et al. used the finite element (FE) method to solve Equations (36) [106]. Recasting the PDEs into a form similar to the transport equations (44) but using physical coordinates, the equations read

$$\begin{cases} \mathbf{V} \cdot \nabla X_i(u, v) - Y_i(u, v) = 0, \\ \mathbf{V} \cdot \nabla Y_i(u, v) - f_i(u, v) = 0, \end{cases} \qquad \begin{aligned} \mathbf{V}^* &= \{V_1 \ \ V_2\} = \{v \ \ f_k(u, v)\}, \\ & i = 1, ..., N;\ i \neq k. \end{aligned} \tag{48}$$

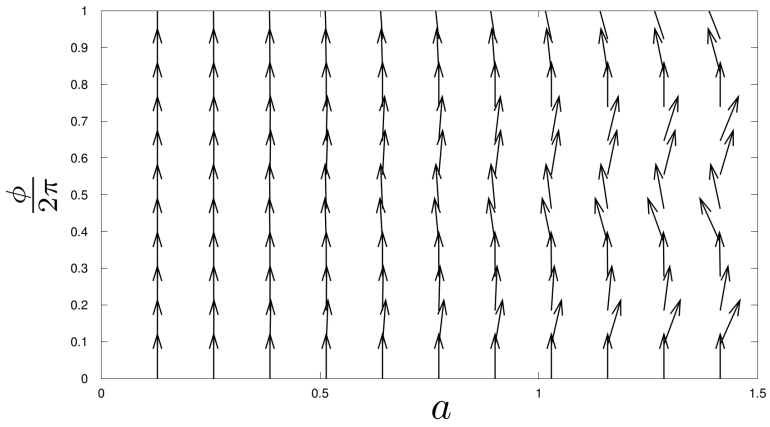

Figure 14: Velocity field of the manifold-governing PDEs in the amplitude-phase domain used by the FDM. Figure reproduced from [104].

These PDEs are quasilinear first-order hyperbolic PDEs bearing strong resemblance to flow equations. Standard Galerkin FE formulations are known to exhibit poor performance in the case of hyperbolic PDEs [111]. The remedy was to employ the streamline upwind Petrov-Galerkin (SUPG) method which proved effective for such problems [112].

Applying a weighted residual approach to Eqs. (48) where the variations $\delta\tilde{Y}_i$ and $\delta\tilde{X}_i$ are considered to preserve consistent units yields

$$\begin{aligned} \int_S \left[\mathbf{V}\cdot\nabla X_i(u,v) - Y_i(u,v)\right]\delta\tilde{Y}_i\, dS = 0, \\ \int_S \left[\mathbf{V}\cdot\nabla Y_i(u,v) - f_i(u,v,\mathbf{X},\mathbf{Y})\right]\delta\tilde{X}_i\, dS = 0, \end{aligned} \tag{49}$$

with $i = 1, ..., N; i \neq k$, and S is the computational domain in the plane (u, v). Within each mesh element e that discretizes S, unknown and virtual fields are expressed as

$$X_i^e = \sum_{b=1}^{\tilde{n}} N^b(u,v) X_i^{e,b} \qquad Y_i^e = \sum_{b=1}^{\tilde{n}} N^b(u,v) Y_i^{e,b} \tag{50}$$

$$\delta\tilde{X}_i^e = \sum_{b=1}^{\tilde{n}} \tilde{N}^b(u,v)\delta\tilde{X}_i^{e,b} \qquad \delta\tilde{Y}_i^e = \sum_{b=1}^{\tilde{n}} \tilde{N}^b(u,v)\delta\tilde{Y}_i^{e,b} \tag{51}$$

where $\tilde{n}$ equals to 3 or 4 for linear triangular or linear quadrangular elements, respectively. The shape functions N^b are first-order Lagrange shape functions. The corresponding test functions are $\tilde{N}^b = N^b + \tau^e \mathbf{V}.\nabla N^b$ where $\tau^e \mathbf{V}.\nabla N^b$ is an upstream overweighting introduced by the SUPG formulation. Note that this upstream overweighting is, in essence, similar to the off-centered finite difference formulation used by Blanc et al. (cf. Section 4.1.2).

Finally, a resolution strategy that grows the invariant manifold from the equilibrium point was developed. Eventually, the manifold was obtained as a collection of annular regions, as illustrated in Figure 15. The successive computational domains were defined using iso-energy curves of the underlying nonlinear conservative system. The continuity between

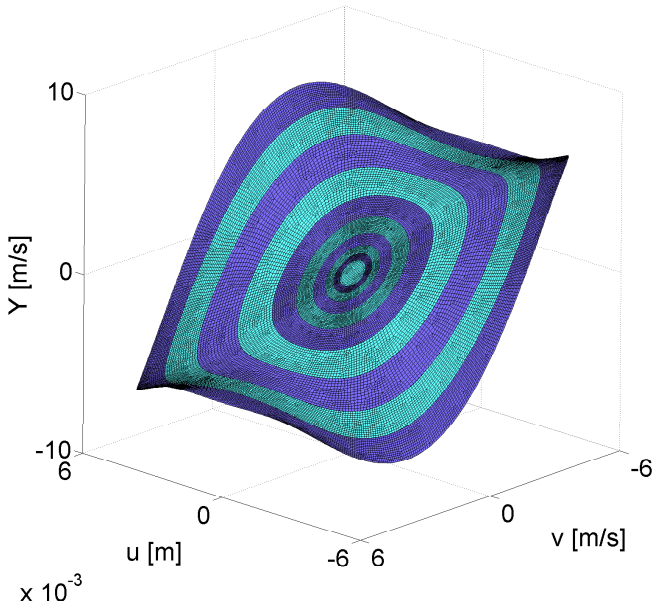

Figure 15: Collection of annular domains forming the invariant manifold in the FE-based method. Figure reproduced from [106].

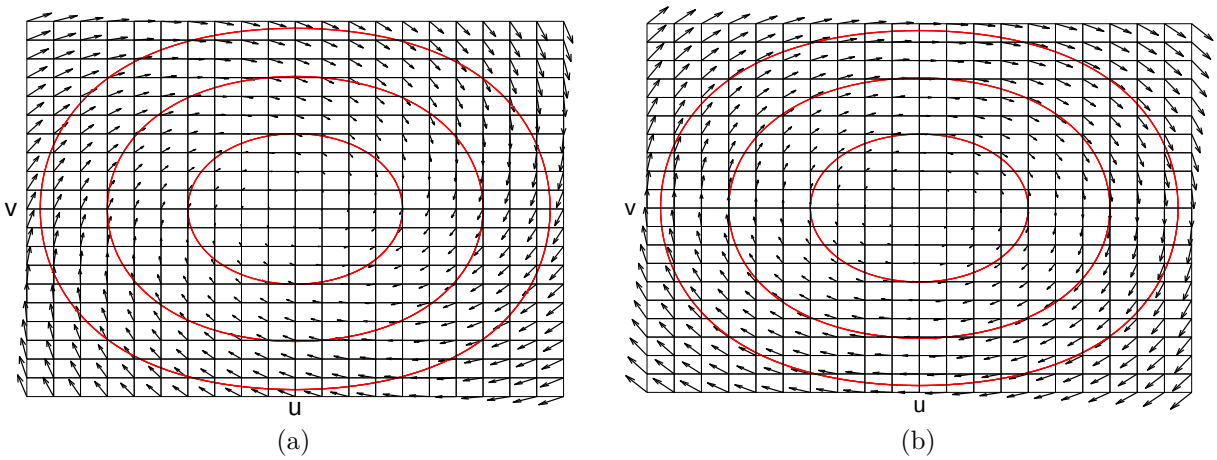

Figure 16: Iso-energy curves (–) and velocity vector $\mathbf{V}$ ($\rightarrow$) for a 2DOF system with cubic nonlinearity. (a) A nonconservative system; (b) a conservative system.

two successive annular regions was naturally ensured by the BCs imposed at inflow. Figure 16 presents in the physical coordinates $(u, v) = (x_1, y_1)$ the PDE velocity field of a 2DOF system with cubic nonlinearity. In the presence of damping (Figure 16(a)), the flow spirals down to the equilibrium point of the system (here, the origin). Considering an annular region defined by two red curves, BCs have to be imposed at the outer boundary, but, for this high-amplitude region, BCs cannot be set before the actual solution is known. However, the flow can be "reversed" by changing the sign of the test functions. Inflow/outflow boundaries are therefore swapped, and the solution computed for the previous annular region can be considered for imposing the desired BCs at the inner

boundary where inflow is now present. Interestingly, for a conservative system, the flow is tangent to the iso-energy curves meaning that no BCs are required (see Figure 16(b)). The method was later generalized by replacing the iso-energy curves by general Lyapunov functions determined using an optimization procedure [113].

4.1.4 Amplitude- and Phase-Dependent Modal Quantities

Another interesting approach was proposed by Bellizzi and Bouc, first for conservative systems [105] and then for nonconservative systems [114]. Similarly to Shaw and Pierre, they defined a NNM motion in terms of a single pair of variables, here, an amplitude and a phase variable $(a(t), \phi(t))$. The other coordinates are functionally related to this pair using the constraint relations

$$\begin{aligned} \mathbf{x}(t) &= a(t)\mathbf{X}(a(t),\phi(t)), \\ \dot{\mathbf{x}}(t) &= \mathbf{y}(t) = a(t)\mathbf{Y}(a(t),\phi(t)), \end{aligned} \tag{52}$$

where $\mathbf{X}$ and $\mathbf{Y}$ are vector functions representing the modal amplitudes. Amplitude and phase variables are described by a pair of ordinary differential equations governing the SDOF motion which takes place on a NNM [114]:

$$\begin{aligned} \dot{\phi}(t) &= \Omega(a(t),\phi(t)), \\ \dot{a}(t) &= a(t)\xi(a(t),\phi(t)). \end{aligned} \tag{53}$$

The scalar functions Ω and ξ govern the motion frequency and damping ratio, respectively. All together, $(\mathbf{X}, \mathbf{Y}, \Omega, \xi)$ define the modal motion.

Substituting Equations (52)–(53) into the equations of motion and removing any explicit time dependence yields the set of PDEs

$$\begin{aligned} \left(\mathbf{X} + a\frac{\partial \mathbf{X}}{\partial a}\right)\xi + \frac{\partial \mathbf{X}}{\partial \phi}\Omega &= \mathbf{Y}, \\ \left(\mathbf{Y} + a\frac{\partial \mathbf{Y}}{\partial a}\right)\xi + \frac{\partial \mathbf{Y}}{\partial \phi}\Omega - \frac{1}{a}\mathbf{f}\left(a\mathbf{X}, a\mathbf{Y}\right) &= \mathbf{0}. \end{aligned} \tag{54}$$

The number of equations in (54) is lower than the number of unknowns by two. Additional normalization conditions are thus added to the set of PDEs.

Equations were then discretized using a Fourier-Galerkin projection similar in principle to the one used by Pesheck et al [108]. In Ref. [115], the resolution strategy was improved to reduce the computational burden associated with this projection. In particular, the *method of lines*, where all but one space dimensions are discretized, was considered to solve equations (54) as an initial value problem.

4.2 Boundary Value Formulations

4.2.1 A Trajectory-Based Method

In the general context of two-dimensional (un)stable invariant manifold calculation, several methods locally grow an invariant surface without assuming any global parametrization as in Eqs. (34). In particular, the method proposed by Doedel et al. [31, 116] solves boundary value problems (BVPs) that define a one-parameter family of trajectories covering the invariant surface. This method was exploited for the computation of damped NNMs in Ref. [113, 117].

Using the general first-order form of the equations of motion, $\dot{\mathbf{z}} = \mathbf{g}(\mathbf{z})$, a trajectory on the invariant manifold is defined as

$$\mathbf{z}'(\tau) = T\mathbf{g}(\mathbf{z}(\tau)), \tag{55}$$

$$\mathbf{z}(0) = \mathbf{z}_E + r_0(\cos(\theta)\boldsymbol{\zeta}_1 + \sin(\theta)\boldsymbol{\zeta}_2), \tag{56}$$

where $(.)'$ denotes the first derivative with respect to the normalized time $\tau \in [0, 1]$, r_0 is a small parameter, and T is the final time. Equations (55)-(56) parametrize using the variable θ a family of trajectories that start on a small ellipse around the equilibrium point $\mathbf{z}_E$. If the vectors $\boldsymbol{\zeta}_1$ and $\boldsymbol{\zeta}_2$ define an eigenplane of the system linearized at $\mathbf{z}_E$, the trajectories describe the corresponding NNM.

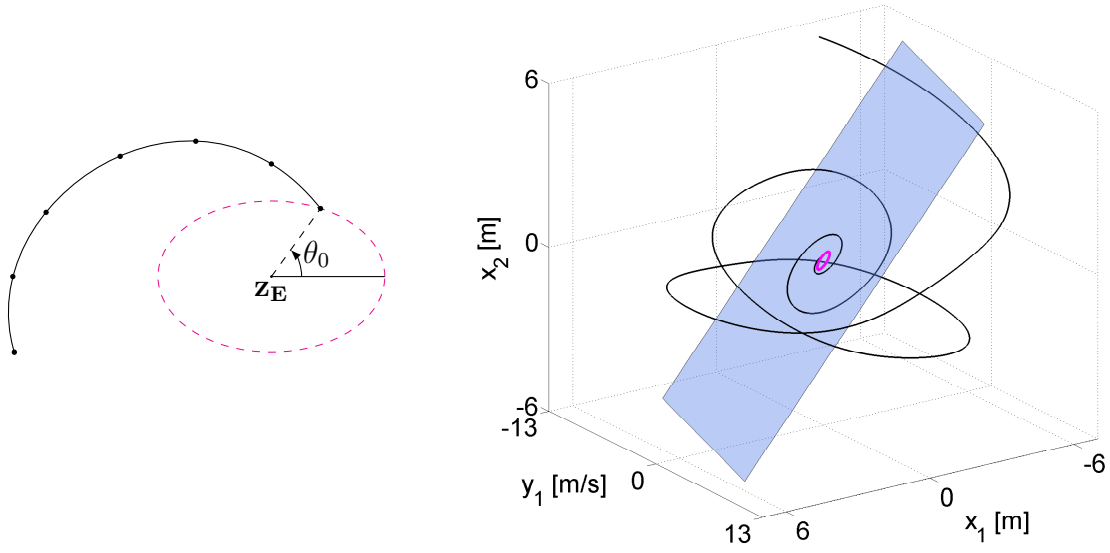

(a) (b)

Figure 17: A first trajectory on the invariant manifold is grown for $\theta = \theta_0$. (a) Schematic representation of the continuation step in the plane (x_1, y_1); (b) complete trajectory in phase space. The small ellipse of ICs (purple) is defined on the tangent space (blue plane) of the NNM using Eq. (56).

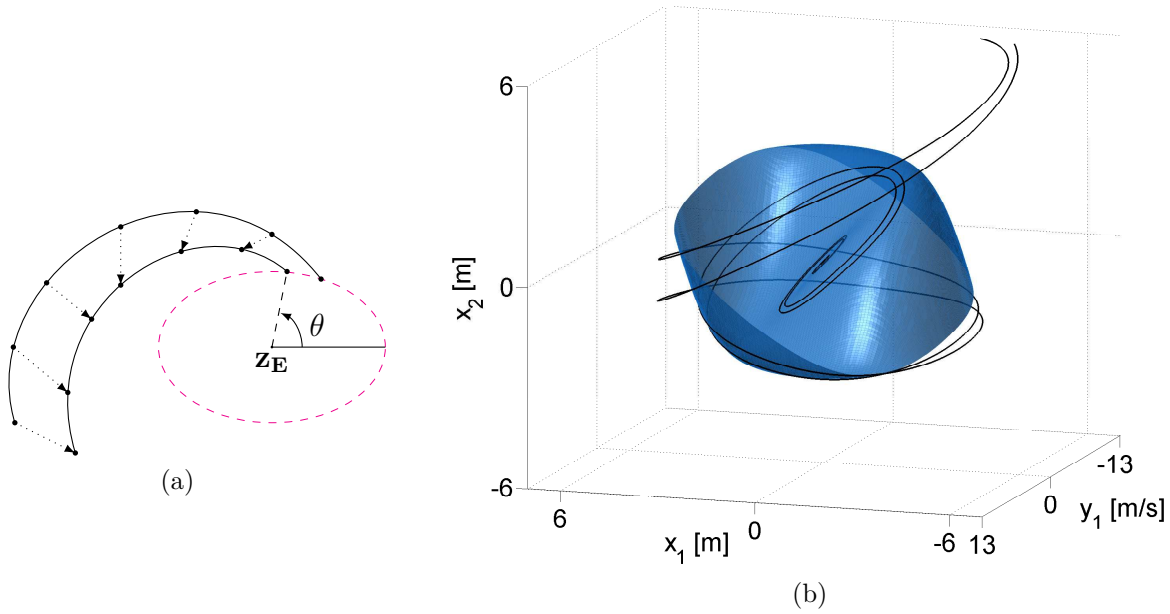

Figure 18: Second continuation step of the trajectory-based approach. Trajectories are continued with respect to θ to cover the entire invariant surface. (a) Schematics of the procedure in the (x_1, y_1) plane; (b) two trajectories on the invariant manifold.

Numerical continuation grows a first trajectory on the manifold with T as free parameter and θ arbitrarily fixed at $\theta = \theta_0$ [118]. Equations (55) are discretized using orthogonal collocation and solved simultaneously for all the points that define the trajectory. This step is illustrated in Figure 17 where, although they can be equally distributed in time, the points along the trajectory are not necessarily equally distributed in space. During the continuation process, a function measuring the arclength of the trajectory as

$$L = \int_0^1 T \, \|\mathbf{g}(\mathbf{z}(l))\| \, dl \tag{57}$$

is monitored by the algorithm, and the continuation is stopped when the trajectory reaches a user-defined length $\bar{L}$. Equation (56) together with the condition $L = \bar{L}$ define a BVP that constrains the initial and final conditions of the trajectory. A second continuation step, during which θ is the parameter and T can freely vary, is then performed, as illustrated in Figure 18. All the points that discretize the first trajectory are continuously varied to compute a second trajectory. The process is repeated for additional trajectories until the invariant surface is adequately covered. We refer to [118] for additional details about the original method.

For a stable system, $T < 0$, and the computation of the first trajectory is similar to backward time integration. The recourse to the BVP approach has however the advantage of being compatible with the subsequent continuation steps. This is a crucial feature of the method because trajectories can be very sensitive with respect to the parameter θ. In addition, the control of the step size in θ with respect to the variation of the entire trajectory guarantees a nice covering of the invariant surface.

4.2.2 The Graph Transform

The graph transform method was used in Ref. [119] in the context of dimension reduction of dynamical systems. The equations of motion $\dot{\mathbf{z}} = \mathbf{g}(\mathbf{z})$ are split into

$$\left\{ \begin{array}{rcl} \dot{\mathbf{u}} & = & \mathbf{g_u}(\mathbf{u}, \mathbf{w}, \lambda), \\ \dot{\mathbf{w}} & = & \mathbf{g_w}(\mathbf{u}, \mathbf{w}, \lambda), \end{array} \right. \tag{58}$$

where $\mathbf{u}$ and $\mathbf{w}$ are the master and slave coordinates, respectively; $\mathbf{g_u}$ and $\mathbf{g_w}$ are the corresponding vector fields, and λ is an artificial parameter.

The method is based on the concept of *overflowing invariant manifold* which can be defined as a compact manifold possessing a boundary where the flow points strictly outward the manifold and for which all trajectories starting inside the manifold remain in it in backward time. Provided that a manifold $\mathcal{M}$ is overflowing invariant, Fenichel's theorem [120] guarantees, under some additional assumptions, the existence of an overflowing invariant manifold $\mathcal{M}^*$ in a perturbed vector field. Following this important theoretical result, the graph transform can be combined with homotopy continuation to turn an initial manifold $\mathcal{M}_0$ into the manifold of the nonlinear system of interest. The computation can thus be initiated without the nonlinearities ($\lambda = 0$), and continuation is used to retrieve the nonlinear system ($\lambda = 1$). Fenichel's theorem guarantees the persistence of the invariant manifold at each continuation step.

The graph transform takes the form

$$\text{graph}(m^{i+1}) = \left(\begin{array}{c} G_u^t \\ G_w^t \end{array} \right) \text{graph}(m^i) \tag{59}$$

where $G_u^t = G_u^t(\mathbf{u}, \mathbf{w})$ and $G_w^t = G_w^t(\mathbf{u}, \mathbf{w})$ represent the flow of Equations (58). The invariant surface is given by

$$\mathcal{M}^i = w^i = \left\{ (\mathbf{u}, \mathbf{w}) \in \mathbb{R}^2 \times \mathbb{R}^{2N-2} | \mathbf{w} = w^i(\mathbf{u}) \right\}, \tag{60}$$

where w^i plays the role of Eqs. (34) and link the slave variables to the master variables. If Fenishel's theorem holds, $w^i \to w^\infty$ as $i \to \infty$ where graph (w^∞) is the unique compact overflowing invariant manifold that satisfies

$$\text{graph}(w^\infty) = \left(\begin{array}{c} G_u^t \\ G_w^t \end{array} \right) \text{graph}(w^\infty) \tag{61}$$

In practice, a uniform grid of points in the set of master coordinates is considered. The idea is to evolve the manifold using the flow of the equations while maintaining an adequate representation (covering) of the invariant surface. To this end, a BVP is defined at each point of the grid. It takes the form of

$$\begin{array}{rcl} G_u^t(\mathbf{u}, \mathbf{w}) - \tilde{\mathbf{u}}_j & = & \mathbf{0}, \\ G_w^t(\mathbf{u}, \mathbf{w}) - w^{i+1}(\tilde{\mathbf{u}}_j) & = & \mathbf{0}, \\ \mathbf{w} - w^i(\mathbf{u}) & = & \mathbf{0}, \end{array} \tag{62}$$

where $\tilde{\mathbf{u}}_j$ is a grid point whose value w^{i+1} is the quantity of interest and ($\mathbf{u}$,$\mathbf{w}$) are unknown. The last two equations give explicitly $w^{i+1}(\tilde{\mathbf{u}}_j)$ and $\mathbf{w}$. The remaining equation is

$$G_u^t(\mathbf{u}, w^i(\mathbf{u})) - \tilde{\mathbf{u}}_j = \mathbf{0}, \tag{63}$$

where $\mathbf{u}$ is unknown. Problem (63) can be solved using classical methods such as shooting or collocation methods. Since the points $\mathbf{u}$ are no longer grid points, the manifold is represented using a tensor-product of cardinal splines with compact support as basis functions $\rho_{j_i}(u_i)$. The manifold reads

$$w(\mathbf{u}) \approx \sum_{j_1=0}^{n_1} \sum_{j_2=0}^{n_2} c_{j_1 j_2} \rho_{j_1}(u_1) \rho_{j_2}(u_2) \tag{64}$$

4.3 Complex Nonlinear Modes

In direct analogy with complex LNMs, complex nonlinear modes were introduced by Laxalde and Thouverez in [121]. The method uses generalized Fourier series to approximate NNM motions and derive a nonlinear eigenvalue problem. More precisely, the complex eigensolutions are written as [121, 122]:

$$\mathbf{x}(t) \approx \mathbf{x}(\gamma, \tau) = \sum_{l=0}^{+\infty} \sum_{m=-\infty}^{+\infty} \hat{\mathbf{x}}_{l,m} e^{-l\gamma + jm\tau} \tag{65}$$

where $\tau = \omega t$ and $\gamma = \beta t$ are two new time scales referring to the fast oscillations and the slow envelope modulations, respectively. Substituting Equation (65) into the equations of motion and using a Fourier-Galerkin projection, a complex eigenvalue problem is obtained:

$$\forall (l,m) \in [0, ..., n_l] \times [-n_m, ..., n_m], \qquad (-l\beta + jm\omega)^2 \hat{\mathbf{x}}_{l,m} - \frac{\langle \mathbf{f}, \rho_{l,m} \rangle}{||\rho_{l,m}||^2} = 0 \tag{66}$$

where $\langle \mathbf{f}, \rho_{l,m} \rangle$ denotes the inner product between $\mathbf{f}$ and the set of basis functions $\rho_{l,m}(\gamma, \tau) = e^{-l\gamma + jm\tau}$. Similarly to the HB method in Section 3.1.2, the nonlinear force vector $\mathbf{f}$ is calculated using an alternating time/frequency approach [50]. $\mathbf{f}$ is thus reconstructed in the time domain using the set $\{\hat{\mathbf{x}}_{l,m}\}$ defining the displacement and velocity vectors. The nonlinear terms are then projected onto the generalized Fourier basis.

The number of unknowns exceeds the number of equation by two [121]. The system is complemented by an additional mode normalization. A control coordinate is selected, and the real and imaginary parts of one of its harmonics are used to define the modal amplitude q as

$$q = q^{\mathcal{R}} + jq^{\mathcal{I}}, \tag{67}$$

where $j^2 = -1$. This complex modal amplitude q represents the two-dimensional subspace on which the NNM motion takes place. Each eigenvector is normalized with respect to q, and the system is solved using Newton-like methods. An alternative normalization based on the kinetic energy was presented in Ref. [123]. Eventually, a continuation algorithm is used to evolve the nonlinear eingenvalue solutions for increasing modal amplitudes.

4.4 Assessment

The first method that was developed for the numerical computation of damped NNMs solves directly the manifold-governing PDEs [108, 109]. This Galerkin-based approach, described in Section 4.1.1, eliminates a number of problems associated with analytical approximations of invariant manifolds. Specifically, it removes the assumption of weakly nonlinear regimes of motion. The accuracy of the results is also reduced to a computational effort and can be guaranteed in the selected computational domain. The PDEs were first discretized using global shape functions resulting in highly-coupled nonlinear algebraic systems that were demanding to solve. The formulation was then improved by considering linear shape functions for the amplitude domain and by solving the PDEs in successive strips. The method was successfully applied to a certain number of conservative systems including a nonlinear beam [108], piecewise-linear systems [124], and rotating systems [125, 126]. Figure 19 depicts the first flapping mode of a rotating beam represented through the slave coordinate corresponding to the second flapping mode. This figure clearly reveals the modal coupling inherent to nonlinear systems that appears when the amplitude increases. The Galerkin-based approach was further generalized to forced systems in Ref. [127]. To the best of our knowledge, the method was applied to damped systems only in a single study [126].

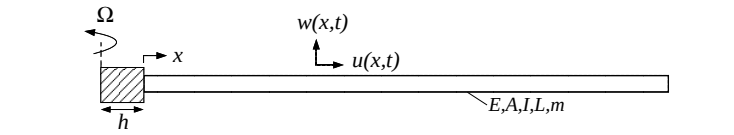

(a)

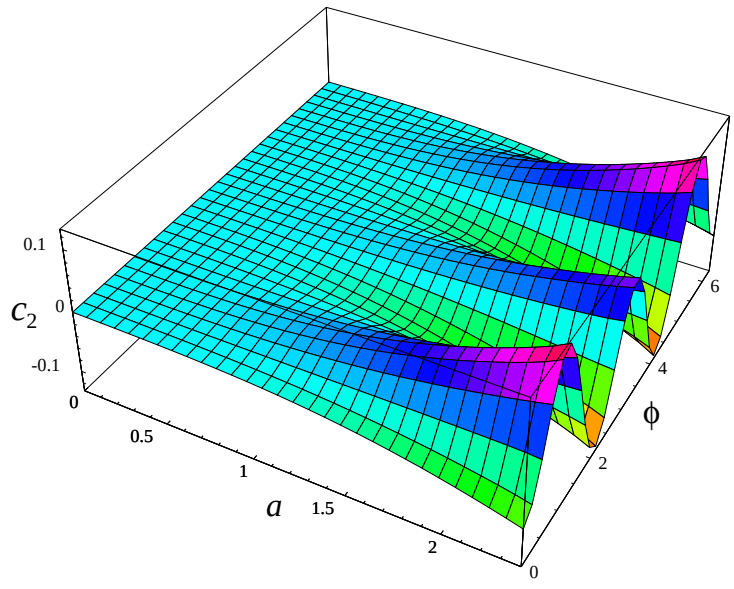

(b)

Figure 19: First flapping NNM of a rotating beam. (a) Schematics of the system; (b) slave modal coordinate c_2 corresponding to the second flapping mode. Figure reproduced from [125].

More recently, the same manifold-governing PDEs were solved using finite differences (Section 4.1.2, [104]). Theoretically sound, the transport method rigorously addresses the hyperbolic nature of the PDEs which was not formally recognized in [108]. The undamped NNMs of a 2DOF system and of a nonlinear beam were computed and used for building reduced-order models (ROMs). Due to the absence of shape functions, there is no direct interpolation basis for computing the dynamics on the invariant manifold, which contrasts with the Galerkin-based approach. Such a basis was computed *a posteriori* by fitting the collection of points of the discretization grid using polynomial functions. We remark that the method in its present form cannot yet be applied to nonconservative systems [104].

The FE-based method also accounts for the hyperbolicity of the PDEs through the streamline upwind Petrov-Galerkin (SUPG) scheme and through the imposition of boundary conditions where inflow is present [106]. The sparse algebraic systems obtained with the FE method combined with a strategy which grows the invariant manifold as a collection of annular regions have further reduced the computational cost compared to the Galerkin-based approach. Overall, these improvements allowed the computation of the NNMs of a model of the Morane-Saulnier aircraft possessing 124 DOFs [113]. The FE method was also applied to several conservative and nonconservative systems with linear and nonlinear damping (including a system of two coupled Van der Pol oscillators [113]) with the advantage that the dynamics on the invariant manifold can be directly interpolated from the FE basis. For illustration, the invariant manifold defining the in-phase NNM of a 2DOF system including regularized Coulomb (RC) friction

$$\begin{aligned} \ddot{x}_1 + (2x_1 - x_2) + F_{\max} \tanh(\kappa \dot{x}_1) &= 0, \\ \ddot{x}_2 + (2x_2 - x_1) &= 0. \end{aligned} \tag{68}$$

is shown in Figure 20(a). $F_{\max} = 1.5\ N$ defines the maximum friction force (at high velocity), and $\kappa = 1\ rad.s/m$ determines the degree of regularization introduced by the hyperbolic tangent function. We note that the method presented some (still unanswered) difficulties for high values of κ. The invariant surface is composed of seven annular regions whose continuity is naturally ensured by the imposed BCs. Figure 20(b) compares the dynamics on the invariant manifold, computed using equations (34) and (37), and the dynamics of the full system. The reduced- and full-system dynamics are in perfect agreement.

In the previous methods, time is eliminated from the manifold-governing PDEs, and the motion frequency has to be identified from the dynamics on the invariant manifold using time-frequency analysis (with, e.g., the Hilbert or wavelet transforms). The method based on amplitude- and phase-dependent modal quantities directly addresses this issue by introducing two additional scalar functions (Ω, ξ) describing the evolution of the frequency and of the damping ratio, respectively (cf. Section 4.1.4). The obtained PDEs were initially solved using a Galerkin method with global shape functions [114], resulting in a prohibitive complexity for increasing system dimensionality. The *method of lines* was found to be a computationally effective alternative and was successfully applied to a clarinet [115]. The construction of a two-dimensional interpolation for integrating in time the dynamics on the NNM is, however, needed because this approach does not exploit shape functions. In particular circumstances, the method presented some divergence issues arguably due to "*some sort of ill-posedness in the equations*" [115].

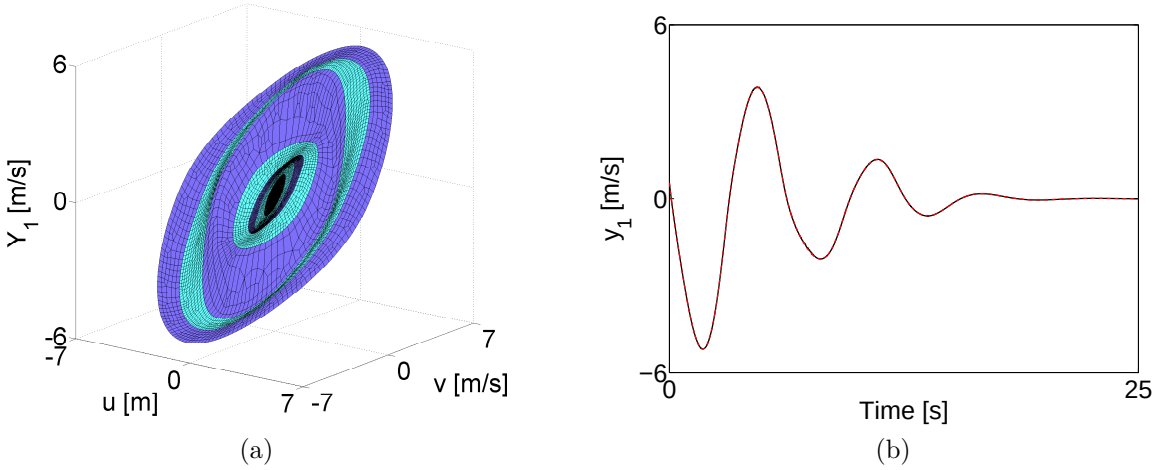

(a) (b)

Figure 20: First NNM of the 2DOF system with regularized Coulomb friction. (a) Invariant surface computed for Y_1 with seven annular domains; (b) comparison between reduced- and full-system dynamics in black and red, respectively. Figure reproduced from [113].

One important assumption with the methods in Section 4.1 is that the invariant manifold can be described using a unique pair of coordinates. However, the invariant manifold defining the in-phase NNM of the 2DOF conservative system (1), shown in Figure 21, presents a complex topology with several foldings which invalidate the chosen parametrization. Even if the selection of appropriate master coordinates plays an important role, it cannot eliminate such foldings which can appear for a number of reasons including internal resonances, localization, and multiple fixed points [104,128–130]. The concept of multi-modal NNMs [128] was then introduced to create multi-mode ROMs accounting for the coupling that may exist between the individual NNMs of interest. The approach is therefore naturally suitable for addressing the presence of internal resonances. The mathematical description of these NNMs is obtained by following the single-mode approach with the difference that n_m pairs of variables are taken as master pairs leading to $2N - 2n_m$ slave variables

$$x_i = X_i\left(\mathbf{u}_m, \mathbf{v}_m\right), \qquad y_i = Y_i\left(\mathbf{u}_m, \mathbf{v}_m\right), \tag{69}$$

where $\mathbf{u}_m$ and $\mathbf{v}_m$ represent the vectors of the nonlinear modal coordinates [128]. After solving the manifold-governing equations in $\mathbb{R}^{2n_m}$, the constraint functionals (69) reduce the dynamics to n_m coupled nonlinear oscillators. The effectiveness of the obtained ROMs was demonstrated in [129] using a nonlinear beam example. An extension of the single-mode method proposed by Pesheck et al. [108] to higher-dimensional PDEs was also presented by Jiang et al. in [130]. Although elegant, this generalization still relies on an explicit and global parametrization of the NNM. Since it does not solve completely the intrinsic parametrization issue, it may therefore fail in other regions of the phase space.

In the trajectory-based method introduced in Section 4.2.1, no parametrization is assumed, which allows to compute NNMs *a priori* without any restriction as to, e.g., the presence of nonlinear modal interactions. The approach was implemented in the software

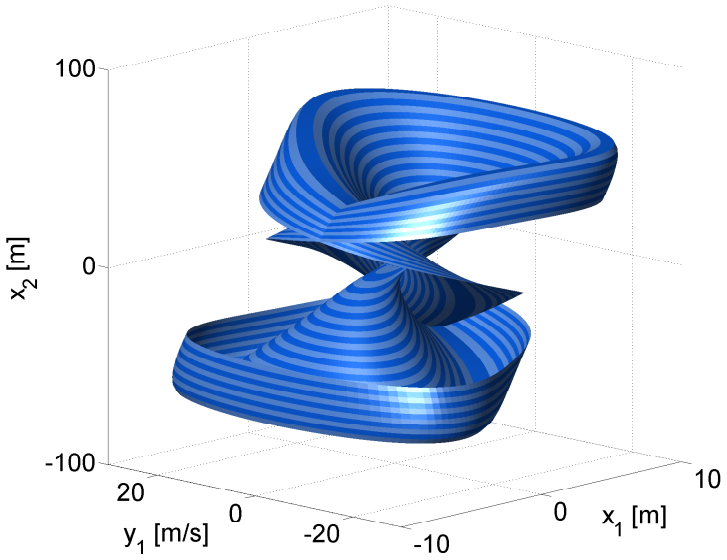

Figure 21: Invariant manifold constructed by gathering in phase space the periodic orbits of the in-phase NNM of the 2DOF conservative system (1). Light- and dark-blue surfaces are built by joining two successive periodic orbits. The surface appears to intersect itself, but this is because the manifold is embedded in a four-dimensional phase space.

AUTO [90], and the manifolds are represented by constructing a mesh between adjacent trajectories. The result obtained for the first mode of the 2DOF system (68) is compared in Figure 22(a) with the solution obtained with the FE-based method. For low to moderate amplitudes, both methods provide manifolds that are in very close agreement. However, owing to the pronounced deformation and folding of the surface, the FE method cannot calculate it for higher amplitudes. The projection in Figure 22(b) of three trajectories onto the plane of master coordinates used by the FE-based approach confirms this observation. The trajectories intersect in two different regions around $(u, v) = (-5, 2)$ and $(u, v) = (2, 5)$, which leads to the failure of the parametrization of the manifold in these regions. The trajectory-based approach is also interesting because it gives the dynamics on the manifold as a byproduct. This valuable information can be analyzed for extracting the frequency-amplitude dependence of the oscillations. An inherent limitation of the method is that it cannot be applied to conservative systems. For lightly-damped systems, a large number of collocation points is required, which significantly increases the computation cost of the method. We also note that the absence of parametrization complicates the construction of a ROM.

The common drawback to the aforementioned methods is that their computational cost directly scales with the codimension of the invariant manifold, i.e., $2N - 2$. Interestingly, the graph transform method presented in Section 4.2.2 scales with the dimension of the invariant manifold, i.e., 2, because the unknown in the BVP problem (63) is $\mathbf{u}$. The method was considered in Ref. [119] to reduce the dynamics of a beam with nonlinear BCs under harmonic excitation. However, the resolution of a BVP for each grid point that discretizes the shape of the manifold can result in an important computational cost. Furthermore, the convergence rate of the method is linear, and it can be influenced by the spectral gap that exists between the different modes of the system [119]. In this context,

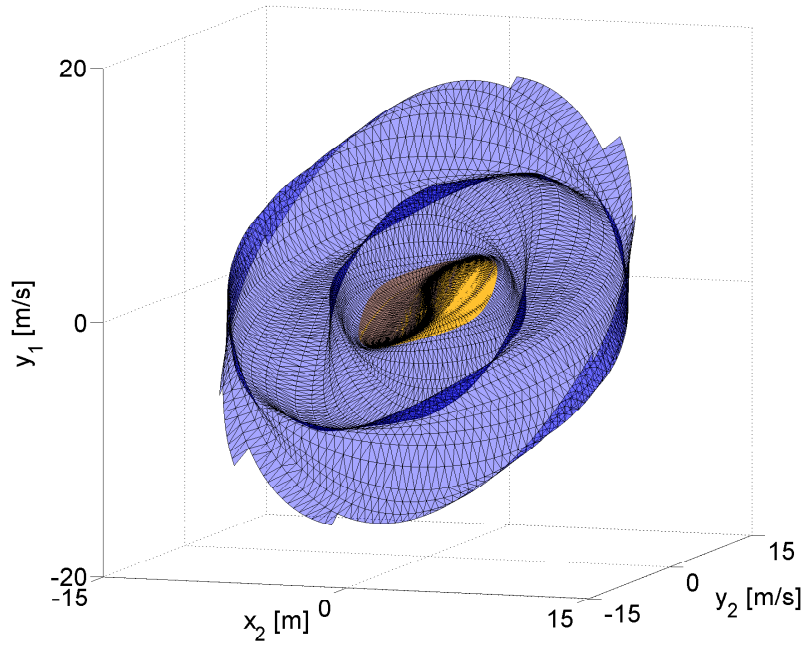

(a)

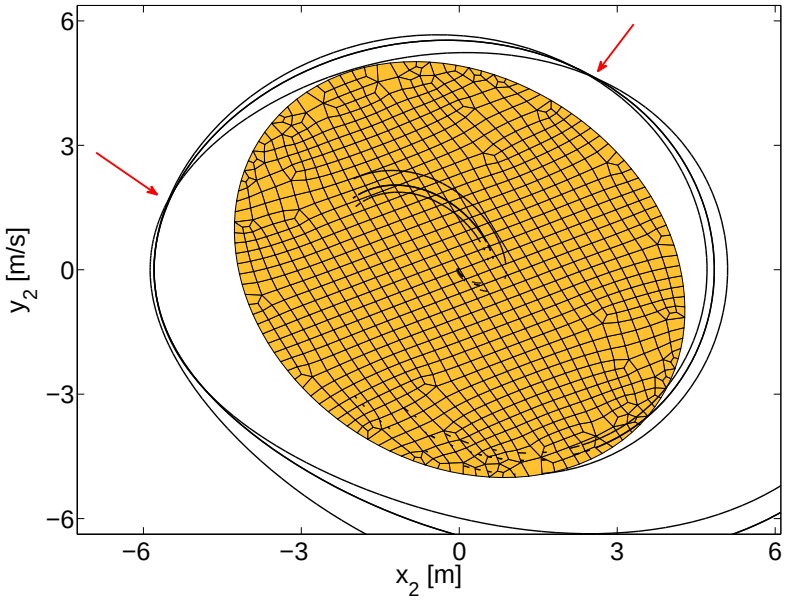

(b)

Figure 22: First NNM of the 2DOF system with regularized Coulomb friction and $F_{max} = 1.5$ N. (a) Trajectory-based method (blue mesh) and FE method (orange mesh); (b) projection of three trajectories (black curves) computed with the trajectory-based approach onto the plane of master coordinates of the FE-based method.

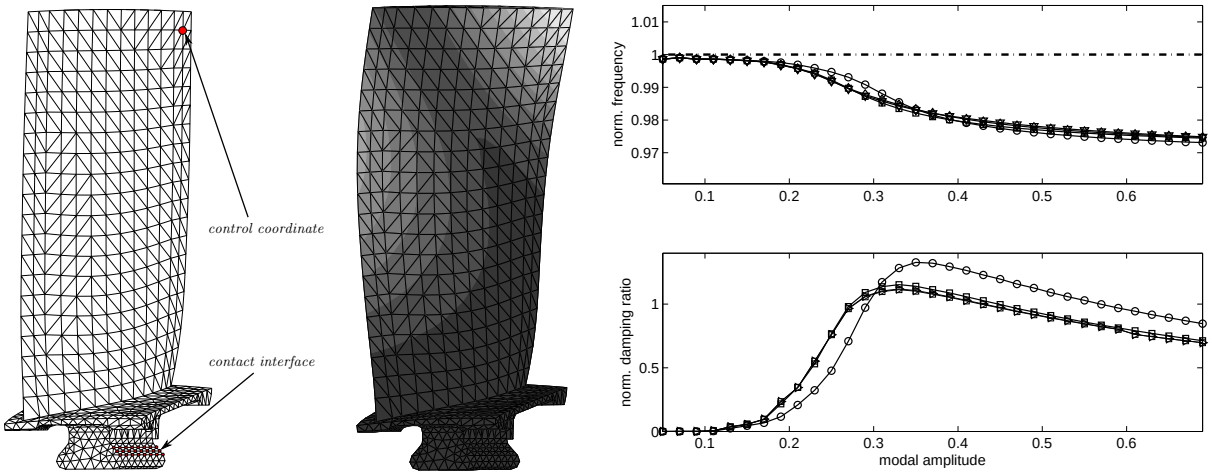

(a) (b) (c)

Figure 23: Complex nonlinear modal analysis of a compressor blade. (a) Finite element model; (b) first torsion mode; (c) evolution of the frequency and damping ratio of the first torsion mode as a function of the modal amplitude q. $(-\circ-)$ one harmonic; $(-\square-)$ three harmonics; $(-\triangledown-)$ five harmonics; $(-\diamond-)$ seven harmonics; $(-.-)$ no-slip. Figure reproduced from [121].

the BVP approach can be replaced by an initial value problem. This approach is very effective, but the evolution of the points that discretize the manifold is difficult to control and can complicate the interpolation with splines. We note that the method considers a set of master variables $\mathbf{u}$ to describe the invariant surface, as a consequence of which the computation remains applicable as far as this parametrization remains valid.

Finally, even if some of the manifold-based methods proved to work for piecewise linear systems, capturing the shape of the invariant surface is increasingly complicated as the system becomes non-regular. In contrast, the direct computation of a trajectory (or a curve) on the invariant surface suffers less from this difficulty. The approach in Section 4.3 approximates trajectories on the invariant surface using generalized Fourier series. This discretization leads to a nonlinear eigenvalue problem that is less expensive to solve than the manifold-governing PDEs. The approach could tackle strongly nonlinear systems of important complexity as, for instance, bladed disks with hysteretic [123] or differential equations [121,131] for modeling the contact interfaces. The compressor blade considered in Ref. [121] is represented in Figure 23(a-b). Figure 23(c) displays the frequency and damping ratio of the first torsion mode, which are a direct outcome of the general Fourier representation. Their evolution as function of the modal amplitude q was captured thanks to continuation. The method was further generalized to address systems with distinct states, i.e., systems where nonlinear forces can be defined piecewise [132]. Because the NNMs are only computed at discrete values of q, linear and piecewise cubic interpolations between the solutions of (66) were proposed [123]. Eventually, a ROM including a single NNM and a set of linearized modes can be synthesized. In Ref. [131], the complex modal quantities were further exploited to derive slow-flow models of the dynamics.

5 Summary and Future Research Directions

Since their introduction in the 1960s by Rosenberg, NNMs have proved useful for understanding the complex dynamics exhibited by nonlinear systems. Specifically, one fundamental property of NNMs is that structural resonances occur in their neighborhood. If analytical approaches were mostly used for NNM calculation until the 1990s, effective computational methods were introduced in the 2000s and were reviewed in the present paper.

The computation of NNMs of large-scale structures with localized stiffness nonlinearities is now within reach. The developed algorithms will enable the practitioner to reveal dynamical phenomena that could be missed otherwise. For instance, the study of the real industrial structures considered in this review supports the claim that interactions between modes with widely-spaced frequencies are generic in structures possessing high modal density. These modal interactions may have important consequences for engineering design, because they can severely increase the response levels endured by the structure. Energy can also be transferred from modes with low effective mass to modes with great effective mass or from out-of-plane modes to in-plane modes, thereby leading to dynamical phenomena unexpected from a linear standpoint. The algorithms can also be used as the first step toward nonlinear model reduction. Even if NNMs cannot be used for modal superposition, single- or multi-mode reduced-order models can be constructed to capture the essential behavior of the system in the vicinity of the considered resonances.

Despite the progress observed in recent years, there remain significant challenges for the computation of NNMs. The following discussion presents some of the key aspects that, we believe, will drive the development of NNMs in the years to come

- The treatment of complex nonlinearities, e.g., nonsmooth nonlinearities and nonlinear hysteretic damping, is still in its infancy. In addition, most real structures investigated so far comprised localized nonlinearities. A step in the direction of geometrically nonlinear structures was presented by Kuether et al. in Ref. [133] where they computed the NNMs of nonlinear beams and plates modeled in commercial finite element codes (see Figure 24).
- Further reduction of the computational burden of existing algorithms should be achieved. The recourse to compiled algorithms adapted to large-scale parallel computation, as in the continuation library LOCA [134], should be attempted. Methods such as the Newton-Picard continuation technique [135], subspace projections [136] and modal derivatives [137] have also the potential to accelerate the computations.
- The detection and rigorous treatment of the bifurcations of NNMs has not been achieved so far. Yet, bifurcations play an important role as they create and eliminate branches of NNMs.
- A spectral characterization of damped NNMs was recently presented in Ref. [138]. Based on the Koopman operator theory, this new mathematical formulation removes manifold parametrization issues, offering new perspectives for computing NNMs in the presence of modal interactions.

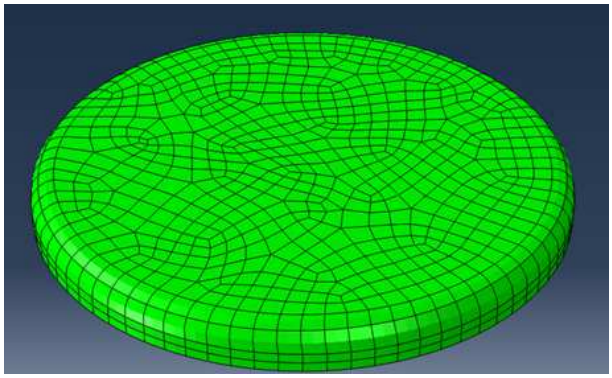

(a)

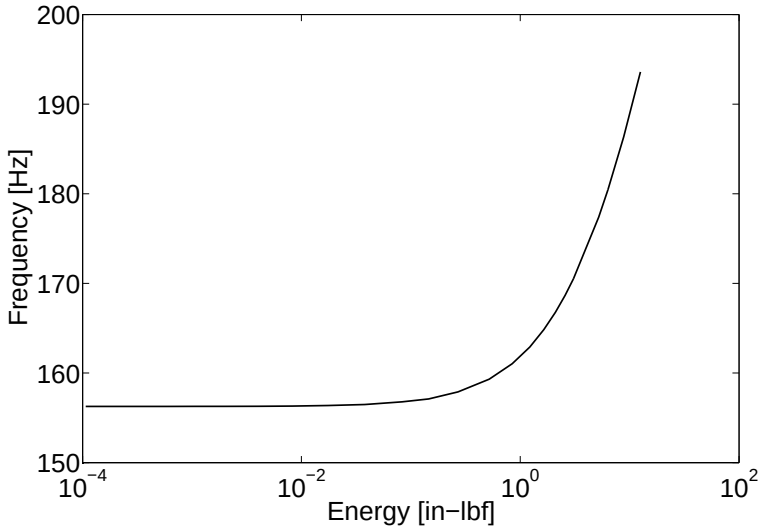

(b)

Figure 24: First NNM of a geometrically nonlinear exhaust cover plate. (a) FE model; (b) FEP. Figure reproduced from [133].

Besides the computational aspects, there are still many open questions regarding the understanding and exploitation of the computed periodic orbits and invariant manifolds:

- The role played by damping in the dynamics of nonlinear structures is not yet completely uncovered. For instance, the question of how modal interactions and invariant manifolds are affected by damping remains largely unanswered.
- Invariant objects play a key role in nonlinear systems and can be seen as attractors of the dynamics. However, the physical information brought by the computation of invariant manifolds has not been fully exploited.
- There have been recent attempts at identifying NNMs from experimental data [139, 140] and at performing continuation in physical experiments [141–143]. Coupling these latter developments with the existing algorithms for NNM computation would pave the way for effective methods for validation of nonlinear structural models.

Acknowledgments

The author L. Renson is Research Fellow (FRIA fellowship) of the *Fonds de la Recherche Scientifique - FNRS*, which is gratefully acknowledged.

References

[1] D. J. Ewins. *Modal Testing: Theory, Practice and Application (2nd Edition)*. Research Studies Press LTD, 2000.

[2] M. Degener. Ground vibration testing for validation of large aircraft structural dynamics. In *Proceedings of the International Forum on Aeroelasticity and Structural Dynamics*, Manchester, UK, 1995.

[3] J. R. Ahlquist, J. M. Carreño, H. Climent, R. de Diego, and J. de Alba. Assessment of nonlinear structural response in A400M GVT. In *Proceedings of the International Modal Analysis Conference, Jacksonville, FL, USA*, 2010.

[4] J. P. Noël, L. Renson, G. Kerschen, B. Peeters, S. Manzato, and J. Debille. Nonlinear dynamic analysis of an F-16 aircraft using GVT data. In *Proceedings of the International Forum on Aeroelasticity and Structural Dynamics, Bristol, UK*, 2013.

[5] N. Boechler, G. Theocharis, and C. Daraio. Bifurcation-based acoustic switching and rectification. *Nature Materials*, 10(9):665–668, 2011. 10.1038/nmat3072.

[6] D. Antonio, D. H. Zanette, and D. Lopez. Frequency stabilization in nonlinear micromechanical oscillators. *Nature Communications*, 3:806, 2012. 10.1038/ncomms1813.

[7] C. M. Donahue, P. W. J. Anzel, L. Bonanomi, T. A. Keller, and C. Daraio. Experimental realization of a nonlinear acoustic lens with a tunable focus. *Applied Physics Letters*, 104(1), 2014.

[8] A. F. Vakakis, O. V. Gendelman, L. A. Bergman, D. M. McFarland, G. Kerschen, and Y. S. Lee. *Nonlinear Targeted Energy Transfer in Mechanical and Structural Systems*, volume 156 of *Solid Mechanics and Its Applications*. Springer Netherlands, 2009.

[9] M. A. Karami and D. J. Inman. Powering pacemakers from heartbeat vibrations using linear and nonlinear energy harvesters. *Applied Physics Letters*, 100(4), 2012.

[10] J. P. Noël, L. Renson, and G. Kerschen. Complex dynamics of a nonlinear aerospace structure: Experimental identification and modal interactions. *Journal of Sound and Vibration*, 333(12):2588–2607, 2014.

[11] A. F. Vakakis, L. I. Manevitch, Y. V. Mlkhlin, V. N. Pilipchuk, and A. A. Zevin. *Normal Modes and Localization in Nonlinear Systems*. Wiley-VCH Verlag GmbH, 2008.

[12] B. Peeters, A. Carrella, J. Lau, M. Gatto, and G. Coppotelli. Advanced shaker excitation signals for aerospace testing. In *Proceedings of the International Modal Analysis Conference (IMAC)*, Jacksonville, USA, 2011.

[13] L. Jezequel and C. H. Lamarque. Analysis of non-linear dynamical systems by the normal form theory. *Journal of Sound and Vibration*, 149(3):429–459, 1991.

[14] A. H. Nayfeh and S. A. Nayfeh. Nonlinear normal modes of a continuous system with quadratic nonlinearities. *Journal of Vibration and Acoustics*, 117(2):199–205, 1995.

[15] O. V. Gendelman. Bifurcations of nonlinear normal modes of linear oscillator with strongly nonlinear damped attachment. *Nonlinear Dynamics*, 37(2):115–128, 2004.

[16] S. Lenci and G. Rega. Dimension reduction of homoclinic orbits of buckled beams via the non-linear normal modes technique. *International Journal of Non-Linear Mechanics*, 42(3):515–528, 2007.

[17] E. L. Allgower and K. Georg. *Introduction to Numerical Continuation Methods*. Classics in Applied Mathematics. SIAM, 2003.

[18] E. J. Doedel. Lecture notes on numerical analysis of nonlinear equations. In B. Krauskopf, H. M. Osinga, and J. Galán-Vioque, editors, *Numerical Continuation Methods for Dynamical Systems*. Springer Netherlands, 2007.

[19] R. Seydel. *Practical Bifurcation and Stability Analysis*, volume 5 of *Interdisciplinary Applied Mathematics*. Springer New York, 2010.

[20] W. J. F. Govaerts. *Numerical Methods for Bifurcations of Dynamical Equilibria*. Society for Industrial and Applied Mathematics, 2000.

[21] H. Dankowicz and F. F. Schilder. *Recipes for Continuation*. Computational Science and Engineering 11, SIAM, 2013.

[22] G. Kerschen, M. Peeters, J. C. Golinval, and A. F. Vakakis. Nonlinear normal modes, part I: A useful framework for the structural dynamicist. *Mechanical Systems and Signal Processing*, 23(1):170–194, 2009.

[23] Y. V. Mikhlin and K. V. Avramov. Nonlinears normal modes for vibrating mechanical systems. review of theoretical developments. *Applied Mechanics Reviews*, 63(6):060802–21, 2010.

[24] K. V. Avramov and Y. V. Mikhlin. Review of applications of nonlinear normal modes for vibrating mechanical systems. *Applied Mechanics Reviews*, 65(2):020801, 2013.

[25] M. Aluko and H.-C. Chang. PEFLOQ: An algorithm for the bifurcational analysis of periodic solutions of autonomous systems. *Computers & Chemical Engineering*, 8(6):355–365, 1984.

[26] M. Holodniok and M. Kubicek. DERPER - an algorithm for the continuation of periodic solutions in ordinary differential equations. *Journal of Computational Physics*, 55(2):254–267, 1984.

[27] C. Franke and C. Führer. Collocation methods for the investigation of periodic motions of constrained multibody systems. *Multibody System Dynamics*, 5(2):133–158, 2001.

[28] E. J. Doedel, R. C. Paffenroth, H. B. Keller, D. J. Dichmann, J. Galï£ · n-Vioque, and A. Vanderbauwhede. Computation of periodic solutions of conservative systems with application to the 3-body problem. *International Journal of Bifurcation and Chaos*, 13(06):1353–1381, 2003.

[29] F. J. Muñoz Almaraz, E. Freire, J. Galán, E. Doedel, and A. Vanderbauwhede. Continuation of periodic orbits in conservative and hamiltonian systems. *Physica D: Nonlinear Phenomena*, 181(1-2):1–38, 2003.

[30] M. Dellnitz and A. Hohmann. A subdivision algorithm for the computation of unstable manifolds and global attractors. *Numerische Mathematik*, 75(3):293–317, 1997.

[31] B. Krauskopf, H. M. Osinga, E. J. Doedel, M. E. Henderson, J. Guckenheimer, A. Vladimirsky, M. Dellnitz, and O. Junge. A survey of methods for computing (un)stable manifolds of vector fields. *International Journal of Bifurcation and Chaos*, 15(3):763–791, 2005.

[32] M. E. Henderson. Computing invariant manifolds by integrating fat trajectories. *SIAM Journal on Applied Dynamical Systems*, 4(4):832–882, 2005.

[33] J. Guckenheimer and A. Vladimirsky. A fast method for approximating invariant manifolds. *SIAM Journal on Applied Dynamical Systems*, 3(3):232–260, 2004.

[34] A. M. Lyapunov. *The general problem of the stability of motion*. Princeton University Press, 1947.

[35] A. Kelley. On the liapounov subcenter manifold. *Journal of Mathematical Analysis and Applications*, 18(3):472–478, 1967.

[36] R. M. Rosenberg. Normal modes of nonlinear dual-mode systems. *Journal of Applied Mechanics*, 27(2):263–268, 1960.

[37] R. M. Rosenberg. The normal modes of nonlinear n-degree-of-freedom systems. *Journal of Applied Mechanics*, 29(1):7–14, 1962.

[38] R. M. Rosenberg. On nonlinear vibrations of systems with many degrees of freedom. *Advances in Applied Mechanics*, 9:155–242, 1966.

[39] Y. S. Lee, G. Kerschen, A. F. Vakakis, P. Panagopoulos, L. Bergman, and D. M. McFarland. Complicated dynamics of a linear oscillator with a light, essentially nonlinear attachment. *Physica D: Nonlinear Phenomena*, 204(1-2):41–69, 2005.

[40] S. W. Shaw and C. Pierre. Non-linear normal modes and invariant manifolds. *Journal of Sound and Vibration*, 150(1):170–173, 1991.

[41] S. W. Shaw and C. Pierre. Normal modes for non-linear vibratory systems. *Journal of Sound and Vibration*, 164:40, 1993.

[42] H. A. Ardeh and M. S. Allen. Instantaneous center manifolds and nonlinear normal modes. In *Proceedings of the ASME 2012 International Design Engineering Technical Conferences & Computers and Information in Engineering Conference*, Chicago, 2012.

[43] H. A. Ardeh and M. S. Allen. Investigating cases of jump phenomenon in a nonlinear oscillatory system. In *Proceedings of the International Modal Analysis Conference (IMAC)*, California, USA, 2013.

[44] M. Peeters, R. Viguié, G. Sérandour, G. Kerschen, and J. C. Golinval. Nonlinear normal modes, part II: Toward a practical computation using numerical continuation techniques. *Mechanical Systems and Signal Processing*, 23(1):195–216, 2009.

[45] R. Arquier, S. Bellizzi, R. Bouc, and B. Cochelin. Two methods for the computation of nonlinear modes of vibrating systems at large amplitudes. *Computers & Structures*, 84(24-25):1565–1576, 2006.

[46] J. C. Simo and N. Tarnow. The discrete energy-momentum method. conserving algorithms for nonlinear elastodynamics. *Zeitschrift für angewandte Mathematik und Physik ZAMP*, 43(5):757–792, 1992.

[47] J. C. Slater. A numerical method for determining nonlinear normal modes. *Nonlinear Dynamics*, 10(1):19–30, 1996.

[48] A. H. Nayfeh and B. Balachandran. *Applied Nonlinear Dynamics, Analytical, Computational, and Experimental Methods*. Wiley-VCH Verlag GmbH, 2007.

[49] S. L. Lau and Y. K. Cheung. Amplitude incremental variational principle for nonlinear vibration of elastic systems. *ASME Journal of Applied Mechanics*, 28:959–964, 1981.

[50] T. M. Cameron and J. H. Griffin. An alternating frequency/time domain method for calculating the steady-state response of nonlinear dynamic systems. *Journal of Applied Mechanics*, 56(1):149–154, 1989.

[51] B. Cochelin and C. Vergez. A high order purely frequency-based harmonic balance formulation for continuation of periodic solutions. *Journal of Sound and Vibration*, 324(1-2):243–262, 2009.

[52] A. Grolet and F. Thouverez. On a new harmonic selection technique for harmonic balance method. *Mechanical Systems and Signal Processing*, 30(0):43–60, 2012.

[53] G. Von Groll and D. J. Ewins. The harmonic balance method with arc-length continuation in rotor/stator contact problems. *Journal of Sound and Vibration*, 241(2):223–233, 2001.

[54] A. Lazarus and O. Thomas. A harmonic-based method for computing the stability of periodic solutions of dynamical systems. *Comptes Rendus Mécanique*, 338(9):510–517, 2010.

[55] H. B. Keller. Numerical solution of bifurcation and nonlinear eigenvalue problems. In P. H. Robinowitz, editor, *Application of Bifurcation Theory: Proceedings of an Advanced Seminar*, 1977.

[56] E. Doedel. Nonlinear Numerics. *J. Franklin Institute*, 334B:1049–1073, 1997.

[57] P. Ribeiro and M. Petyt. Non-linear free vibration of isotropic plates with internal resonance. *International Journal of Non-Linear Mechanics*, 35(2):263–278, 2000.

[58] B. Cochelin. A path-following technique via an asymptotic-numerical method. *Computers & Structures*, 53(5):1181–1192, 1994.

[59] B. Cochelin, N. Damil, and M. Potier-Ferry. Asymptotic-numerical methods and Pade approximants for non-linear elastic structures. *International Journal for Numerical Methods in Engineering*, 37(7):1187–1213, 1994.

[60] B. Cochelin, N. Damil, and M. Potier-Ferry. *Méthode Asymptotique Numérique (in french)*. Hermès - Lavoisier, 2007.

[61] P. Vannucci, B. Cochelin, N. Damil, and M. Potier-Ferry. An asymptotic-numerical method to compute bifurcating branches. *International Journal for Numerical Methods in Engineering*, 41(8):1365–1389, 1998.

[62] S. Baguet and B. Cochelin. On the behaviour of the anm continuation in the presence of bifurcations. *Communications in Numerical Methods in Engineering*, 19(6):459–471, 2003.

[63] B. Cochelin and M. Medale. Power series analysis as a major breakthrough to improve the efficiency of asymptotic numerical method in the vicinity of bifurcations. *Journal of Computational Physics*, 236(0):594–607, 2013.

[64] R. J. Kuether, L. Renson, T. Detroux, C. Grappasonni, G. Kerschen, and M. S. Allen. Nonlinear normal modes, modal interactions and isolated resonance curves. *Journal of Sound and Vibration*, 351:299–310, 2015.

[65] S. Tsakirtzis, P. N. Panagopoulos, G. Kerschen, O. Gendelman, A. F. Vakakis, and L. A. Bergman. Complex dynamics and targeted energy transfer in linear oscillators coupled to multi-degree-of-freedom essentially nonlinear attachments. *Nonlinear Dynamics*, 48(3):285–318, 2006.

[66] G. Kerschen, J. J. Kowtko, D. M. McFarland, L. A. Bergman, and A. F. Vakakis. Theoretical and experimental study of multimodal targeted energy transfer in a system of coupled oscillators. *Nonlinear Dynamics*, 47(1-3):285–309, 2006.

[67] F. Georgiades, M. Peeters, G. Kerschen, J. C. Golinval, and M. Ruzzene. Modal analysis of a nonlinear periodic structure with cyclic symmetry. *AIAA Journal*, 47(4):1014–1025, 2009.

[68] K. R. Jayaprakash, Y. Starosvetsky, A. F. Vakakis, M. Peeters, and G. Kerschen. Nonlinear normal modes and band zones in granular chains with no pre-compression. *Nonlinear Dynamics*, 63(3):359–385, 2011.

[69] G. Kerschen, M. Peeters, J. C. Golinval, and C. Stéphan. Nonlinear modal analysis of a full-scale aircraft. *Journal of Aircraft*, 50(5):1409–1419, 2013.

[70] L. Renson, J. P. Noël, and G. Kerschen. Complex dynamics of a nonlinear aerospace structure: numerical continuation and normal modes. *Nonlinear Dynamics*, 79(2):1293–1309, 2015.

[71] M. Peeters, G. Kerschen, and J. C. Golinval. Dynamic testing of nonlinear vibrating structures using nonlinear normal modes. *Journal of Sound and Vibration*, 330(3):486–509, 2011.

[72] R. J. Kuether and M. S. Allen. Computing nonlinear normal modes using numerical continuation and force appropriation. In *Proceedings of the ASME 2012 International Design Engineering Technical Conferences & Computers and Information in Engineering Conference*, Chicago, 2012.

[73] F. Wang, A. K. Bajaj, and K. Kamiya. Nonlinear normal modes and their bifurcations for an inertially coupled nonlinear conservative system. *Nonlinear Dynamics*, 42:33, 2005.

[74] F. Wang and A. Bajaj. Nonlinear normal modes in multi-mode models of an inertially coupled elastic structure. *Nonlinear Dynamics*, 47(1):25–47, 2007.

[75] T. Detroux, L. Renson, and G. Kerschen. The harmonic balance method for advanced analysis and design of nonlinear mechanical system. In *Proceedings of the International Modal Analysis Conference, Orlando, USA*, 2014.

[76] B. Zhou, F. Thouverez, and D. Lenoir. Essentially nonlinear piezoelectric shunt circuits applied to mistuned bladed disks. *Journal of Sound and Vibration*, 333(9):2520–2542, 2014.

[77] E. Sarrouy, A. Grolet, and F. Thouverez. Global and bifurcation analysis of a structure with cyclic symmetry. *International Journal of Non-Linear Mechanics*, 46(5):727–737, 2011.

[78] A. Grolet and F. Thouverez. Free and forced vibration analysis of a nonlinear system with cyclic symmetry: Application to a simplified model. *Journal of Sound and Vibration*, 331(12):2911–2928, 2012.

[79] J. Shao and B. Cochelin. Theoretical and numerical study of targeted energy transfer inside an acoustic cavity by a non-linear membrane absorber. *International Journal of Non-Linear Mechanics*, 64(0):85–92, 2014.

[80] R. Lewandowski. Computational formulation for periodic vibration of geometrically nonlinear structures - part 2: Numerical strategy and examples. *International Journal of Solids and Structures*, 34(15):1949–1964, 1997.

[81] P. Ribeiro and M. Petyt. Nonlinear vibration of plates by the hierarchical finite element and continuation methods. *International Journal of Mechanical Sciences*, 41(4-5):437–459, 1999.

[82] S. Stoykov and P. Ribeiro. Periodic geometrically nonlinear free vibrations of circular plates. *Journal of Sound and Vibration*, 315(3):536–555, 2008.

[83] S. Stoykov and P. Ribeiro. Nonlinear free vibrations of beams in space due to internal resonance. *Journal of Sound and Vibration*, 330(18-19):4574–4595, 2011.

[84] R. Lewandowski. Non-linear free vibrations of beams by the finite element and continuation methods. *Journal of Sound and Vibration*, 170(5):577–593, 1994.

[85] S. Karkar. *Numerical Methods for nonlinear dynamical systems. Application to self-sustained oscillations in musical instruments*. PhD thesis, Laboratoire de Mécanique et d'acoustique, 2012.

[86] S. Karkar, C. Vergez, and B. Cochelin. Numerical tools for musical instruments acoustics: analysing nonlinear physical models using continuation of periodic solutions. In *Proceedings of Acoustics 2012*, Nantes, France, 2012.

[87] E. H. Moussi, S. Bellizzi, B. Cochelin, and I. Nistor. Nonlinear normal modes of a two degrees-of-freedom piecewise linear system. *Mechanical Systems and Signal Processing*, 64-65(0):266–281, 2015.

[88] MHI. Root cause analysis report for tube wear identified in the unit 2 and unit 3 steam generators of San Onofre nuclear generating station, NRC, 2013.

[89] S. Karkar, B. Cochelin, and C. Vergez. A comparative study of the harmonic balance method and the orthogonal collocation method on stiff nonlinear systems. *Journal of Sound and Vibration*, 333(12):2554–2567, 2014.

[90] E. J. Doedel, R. C. Paffenroth, A. R. Champneys, T. F. Fairgrieve, Y. A. Kuznetsov, B. E. Oldeman, B. Sandstede, and X. J. Wang. Auto2000: Continuation and bifurcation software for ordinary differential equations, 2000. available via *http://cmvl.cs.concordia.ca/*.

[91] A. Dhooge, W. Govaerts, and Y. A. Kuznetsov. Matcont: A matlab package for numerical bifurcation analysis of odes. *ACM Trans. Math. Softw.*, 29(2):141–164, 2003.

[92] G. Sérandour, M. Peeters, G. Kerschen, and J.C. Golinval. Computation of nonlinear normal modes, part II: Numerical continuation in auto. In *Proceedings of the ENOC*, Saint Petersburg, Russia, 2008.

[93] M. Ducceschi, C. Touzé, S. Bilbao, and C. J. Webb. Nonlinear dynamics of rectangular plates: investigation of modal interaction in free and forced vibrations. *Acta Mechanica*, pages 1–20, 2013.

[94] NNMcont - A matlab package for the computation of nonlinear normal modes. http://www.ltas-vis.ulg.ac.be/cmsms/index.php?page=nnm#package, 2014.

[95] M. Jerschl, D. Süß, and K. Willner. Numerical continuation methods for the concept of non-linear normal modes. In *Proceedings of the International Modal Analysis Conference (IMAC)*, Orlando, USA, 2014.

[96] L. Azrar, B. Cochelin, N. Damil, and M. Potier-Ferry. An asymptotic-numerical method to compute the postbuckling behaviour of elastic plates and shells. *International Journal for Numerical Methods in Engineering*, 36(8):1251–1277, 1993.

[97] J. M. Cadou, M. Potier-Ferry, B. Cochelin, and N. Damil. Anm for stationary Navier-Stokes equations and with Petrov-Galerkin formulation. *International Journal for Numerical Methods in Engineering*, 50(4):825–845, 2001.

[98] J. M. Cadou, M. Potier-Ferry, and B. Cochelin. A numerical method for the computation of bifurcation points in fluid mechanics. *European Journal of Mechanics - B/Fluids*, 25(2):234–254, 2006.

[99] Manlab - An interactive path-following and bifurcation analysis software. http://manlab.lma.cnrs-mrs.fr/, 2012.

[100] I. Charpentier. On higher-order differentiation in nonlinear mechanics. *Optimization Methods and Software*, 27(2):221–232, 2011.

[101] T. D Burton. Numerical calculation of nonlinear normal modes in structural systems. *Nonlinear Dynamics*, 49(3):425–441, 2007.

[102] D. Laxalde and M. Legrand. Nonlinear modal analysis of mechanical systems with frictionless contact interfaces. *Computational Mechanics*, 47(4):469–478, 2011.

[103] C. Touzé and M. Amabili. Nonlinear normal modes for damped geometrically nonlinear systems: Application to reduced-order modelling of harmonically forced structures. *Journal of Sound and Vibration*, 298(4-5):958–981, 2006.

[104] F. Blanc, C. Touzé, J. F. Mercier, K. Ege, and A. S. Bonnet Ben-Dhia. On the numerical computation of nonlinear normal modes for reduced-order modelling of conservative vibratory systems. *Mechanical Systems and Signal Processing*, 36(2):520–539, 2013.

[105] S. Bellizzi and R. Bouc. A new formulation for the existence and calculation of nonlinear normal modes. *Journal of Sound and Vibration*, 287(3):545–569, 2005.

[106] L. Renson, G. Deliége, and G. Kerschen. An effective finite-element-based method for the computation of nonlinear normal modes of nonconservative systems. *Meccanica*, 49(8):1901–1916, 2014.

[107] J. Carr. *Applications of Centre Manifold Theory*, volume 35 of *Applied Mathematical Sciences*. Springer-Verlag, 1981.

[108] E. Pesheck, C. Pierre, and S. W. Shaw. A new Galerkin-based approach for accurate non-linear normal modes through invariant manifolds. *Journal of Sound and Vibration*, 249(5):971–993, 2002.

[109] E. Pesheck. *Reduced order modeling of nonlinear structural systems using nonlinear normal modes and invariant manifolds*. PhD thesis, University of Michigan, 2000.

[110] J.-L. Lions. *Optimal Control of Systems Governed by Partial Differential Equations*. Springer-Verlag, 1971.

[111] A. Ern and J.-L. Guermond. *Theory and Practice of Finite Elements*, volume 159 of *Applied Mathematical Sciences*. Springer New York, 2004.

[112] A. N. Brooks and T. J. R. Hughes. Streamline upwind/Petrov-Galerkin formulations for convection dominated flows with particular emphasis on the incompressible Navier-Stokes equations. *Computer Methods in Applied Mechanics and Engineering*, 32(1-3):199–259, 1982.

[113] L. Renson. *Nonlinear Modal Analysis of Conservative and Nonconservative Aerospace Structures*. PhD thesis, Aerospace and Mechanical Engineering, Liège, 2014.

[114] S. Bellizzi and R. Bouc. An amplitude-phase formulation for nonlinear modes and limit cycles through invariant manifolds. *Journal of Sound and Vibration*, 300(3-5):896–915, 2007.

[115] D. Noreland, S. Bellizzi, C. Vergez, and R. Bouc. Nonlinear modes of clarinet-like musical instruments. *Journal of Sound and Vibration*, 324(3-5):983–1002, 2009.

[116] E. J. Doedel, B. Krauskopf, and H. M. Osinga. Global bifurcations of the lorenz manifold. *Nonlinearity*, 19, 2006.

[117] L. Renson, C. Touzé, and G. Kerschen. Computation of damped nonlinear normal modes with internal resonances: a boundary value approach. In *Proceedings of the ENOC*, Vienna, Austria, 2014.

[118] B. Krauskopf and H. M. Osinga. Computing invariant manifolds via the continuation of orbit segments. In B. Krauskopf, H. M. Osinga, and J. Galán-Vioque, editors, *Numerical Continuation Methods for Dynamical Systems*. Springer Netherlands, 2007.

[119] M. Elmegard. *Mathematical Modeling and Dimension Reduction in Dynamical Systems*. PhD thesis, 2014.

[120] S. Wiggins. *Normally Hyperbolic Invariant Manifolds in Dynamical Systems*, volume 105 of *Applied Mathematical Sciences*. Springer-Verlag, 1994.

[121] D. Laxalde and F. Thouverez. Complex non-linear modal analysis for mechanical systems: Application to turbomachinery bladings with friction interfaces. *Journal of Sound and Vibration*, 322(4-5):1009–1025, 2009.

[122] D. Laxalde, L. Salles, L. Blanc, and F. Thouverez. Non-linear modal analysis for bladed disks with friction contact interfaces. In *Proceedings of GT2008, ASME Turbo Expo 2008: Power for Land, Sea and Air, Berlin, Germany*, 2008.

[123] M. Krack, L. Panning-von Scheidt, and J. Wallaschek. A method for nonlinear modal analysis and synthesis: Application to harmonically forced and self-excited mechanical systems. *Journal of Sound and Vibration*, 332(25):6798–6814, 2013.

[124] D. Jiang, C. Pierre, and S. W. Shaw. Large-amplitude non-linear normal modes of piecewise linear systems. *Journal of Sound and Vibration*, 272(3-5):869–891, 2004.

[125] E. Pesheck, C. Pierre, and S. W. Shaw. Accurate reduced-order models for a simple rotor blade model using nonlinear normal modes. *Mathematical and Computer Modelling*, 33(10-11):1085–1097, 2001.

[126] M. Legrand, D. Jiang, C. Pierre, and S. W. Shaw. Nonlinear normal modes of a rotating shaft based on the invariant manifold method. *International Journal of Rotating Machinery*, 10(4):319–335, 2004.

[127] D. Jiang, C. Pierre, and S. W. Shaw. Nonlinear normal modes for vibratory systems under harmonic excitation. *Journal of Sound and Vibration*, 288(4-5):791–812, 2005.

[128] N. Boivin, C. Pierre, and S. W. Shaw. Non-linear modal analysis of structural systems featuring internal resonances. *Journal of Sound and Vibration*, 182:6, 1995.

[129] E. Pesheck, N. Boivin, C. Pierre, and S. W. Shaw. Nonlinear modal analysis of structural systems using multi-mode invariant manifolds. *Nonlinear Dynamics*, 25, 2001.

[130] D. Jiang, C. Pierre, and S. W. Shaw. The construction of non-linear normal modes for systems with internal resonance. *International Journal of Non-Linear Mechanics*, 40(5):729–746, 2005.

[131] M. Krack, L. Panning-von Scheidt, and J. Wallaschek. On the computation of the slow dynamics of nonlinear modes of mechanical systems. *Mechanical Systems and Signal Processing*, 42(1-2):71–87, 2014.

[132] M. Krack, L. Panning-von Scheidt, and J. Wallaschek. A high-order harmonic balance method for systems with distinct states. *Journal of Sound and Vibration*, 332(21):5476–5488, 2013.

[133] R. J. Kuether and M. S. Allen. A numerical approach to directly compute nonlinear normal modes of geometrically nonlinear finite element models. *Mechanical Systems and Signal Processing*, 46(1):1–15, 2014.

[134] LOCA - Library of continuation algorithms. http://www.cs.sandia.gov/LOCA/, 2014.

[135] K. Lust and D. Roose. An adaptive Newton–Picard algorithm with subspace iteration for computing periodic solutions. *SIAM Journal on Scientific Computing*, 19(4):1188–1209, 1998.

[136] D. Bindel, M. Friedman, W. Govaerts, J. Hughes, and Y. A. Kuznetsov. Numerical computation of bifurcations in large equilibrium systems in Matlab. *Journal of Computational and Applied Mathematics*, 261(0):232–248, 2014.

[137] F. Wenneker and P. Tiso. *A Substructuring Method for Geometrically Nonlinear Structures*, chapter 14, pages 157–165. Conference Proceedings of the Society for Experimental Mechanics Series. Springer International Publishing, 2014.

[138] G. I. Cirillo, A. Mauroy, L. Renson, G. Kerschen, and R. Sepulchre. Global parametrization of the invariant manifold defining nonlinear normal modes using the koopman operator. In *Proceedings of the ASME 2015 International Design Engineering Technical Conferences & Computers and Information in Engineering Conference*, Boston, 2015.

[139] M. Peeters, G. Kerschen, and J. C. Golinval. Modal testing of nonlinear vibrating structures based on nonlinear normal modes: Experimental demonstration. *Mechanical Systems and Signal Processing*, 25(4):1227–1247, 2011.

[140] J. P. Noël, L. Renson, C. Grappasonni, and G. Kerschen. Identification of nonlinear normal modes of engineering structures under broadband forcing. *Mechanical Systems and Signal Processing, in press, http://dx.doi.org/10.1016/j.ymssp.2015.04.016.*

[141] D. A. W. Barton and S. G. Burrow. Numerical continuation in a physical experiment: Investigation of a nonlinear energy harvester. *Journal of Computational and Nonlinear Dynamics*, 6(1), 2010.

[142] D. A. W. Barton, B. P. Mann, and S. G. Burrow. Control-based continuation for investigating nonlinear experiments. *Journal of Vibration and Control*, 18(4):509–520, 2012.

[143] E. Bureau, F. Schilder, I. Ferreira Santos, J. J. Thomsen, and J. Starke. Experimental bifurcation analysis of an impact oscillator - tuning a non-invasive control scheme. *Journal of Sound and Vibration*, 332(22):5883–5897, 2013.